

Artificial Muscles: Mechanisms, Applications, and Challenges

Seyed M. Mirvakili* and Ian W. Hunter

The area of artificial muscle is a highly interdisciplinary field of research that has evolved rapidly in the last 30 years. Recent advances in nanomaterial fabrication and characterization, specifically carbon nanotubes and nanowires, have had major contributions in the development of artificial muscles. However, what can artificial muscles really do for humans? This question is considered here by first examining nature's solutions to this design problem and then discussing the structure, actuation mechanism, applications, and limitations of recently developed artificial muscles, including highly oriented semicrystalline polymer fibers; nanocomposite actuators; twisted nanofiber yarns; thermally activated shape-memory alloys; ionic-polymer/metal composites; dielectric-elastomer actuators; conducting polymers; stimuli-responsive gels; piezoelectric, electrostrictive, magnetostrictive, and photostrictive actuators; photoexcited actuators; electrostatic actuators; and pneumatic actuators.

1. Introduction

Artificial muscle is a generic term for a class of materials and devices that can reversibly contract, expand, or rotate within one component due to an external stimulus (such as voltage, current, pressure, temperature, light, etc.).^[1] The three basic actuation responses – contraction, expansion, and rotation – can be combined within a single component to produce other types of motions (e.g., bending, by contracting one side of the material while expanding the other side).^[1] The field of artificial muscle is highly interdisciplinary and overlaps with various fields such as material science, chemical engineering, mechanical engineering, electrical engineering, and chemistry. Here, we focus primarily on the scientific aspects of artificial muscles that have been developed recently and do not discuss the artificially made biological muscles for *in vivo* use in human body. Therefore, the terms “artificial muscle” and “actuator” are interchangeably used. Topics on dynamic modeling, device design, and control system design are excluded. Deeper insights into the working mechanism, manufacturing processes, and mathematical modeling of artificial muscles can be obtained by

referencing comprehensive review books and articles on different categories of artificial muscles.^[2–4]

We start by defining some of the common metrics used in the field for measuring the performance of artificial muscles. The definitions are:

Output Strain (ϵ): The change in length upon excitation normalized to the initial length.

Output Stress (σ): The generated force upon excitation normalized to the initial cross-sectional area of the muscle at rest (engineering stress, σ_E) or at the excited state (true stress, σ_T).

Energy (Work) Density (W): The output work generated by the muscle upon excitation normalized to the mass or volume of the muscle. The volumetric energy density can be evaluated by $W = \epsilon \times \sigma_E$. For biological muscles and in general muscles with rhythmic activities, the work-loop method gives a more accurate estimate of the work density (see the Supporting Information).

Power Density (P): The energy (work) density normalized to the actuation period.

Catch-State (Lock-Up State): When an actuator holds its actuated state without consuming any energy. Muscles of some aquatic organisms such mollusks exhibit a catch-state (they hold the shell locked without consuming energy).

Actuation Directionality: Unidirectional, the ability to actively contract (e.g., muscle, solenoid) or expand in length; bidirectional, the ability to actively contract and expand (e.g., Lorentz force actuators).

Cycle Life: The number of cycles an artificial muscle can survive before failure.

Efficiency (η): The ratio of output work over input energy (the input energy can be in the form of electricity, heat, radiation, etc.).

Bandwidth: The range of frequencies that the actuator can be excited continuously.

It is important to note that the magnitude of the stimulus (e.g., voltage, current, heat, etc.) is also an important parameter in selecting the best suited actuator for a specific application.

2. Biological Muscle and Its Properties

To better appreciate the performance of different artificial muscle technologies, biological muscles are discussed here

Dr. S. M. Mirvakili, Prof. I. W. Hunter
BioInstrumentation Laboratory, Department
of Mechanical Engineering
Massachusetts Institute of Technology
Cambridge, MA 02139, USA
E-mail: seyed@mit.edu, sm.mirvakili@gmail.com

 The ORCID identification number(s) for the author(s) of this article can be found under <https://doi.org/10.1002/adma.201704407>.

DOI: [10.1002/adma.201704407](https://doi.org/10.1002/adma.201704407)

first. Muscle consists of a bundle of muscle fibers (single cells). Each muscle fiber (20–200 μm diameter) consists of myofilaments which are in turn comprised of the contractile proteins (including actin, myosin, tropomyosin, and troponin). These proteins are organized in a contractile unit called the sarcomere (typically around 2 μm long) which consists of ≈ 300 myosin molecules. The heads of the myosin molecules (called cross-bridges) attach sequentially to adjacent actin molecules, generating forces in the piconewton range. Sequential attachment and detachment of these cross-bridges powered by the energy contained in the third phosphate bond of adenosine triphosphate (ATP) generates actuation. This molecular contractile mechanism is turned on by action potentials initiated by the neural input to the muscle fiber. Muscle is an example of a linear molecular stepping motor under the control of the nervous system. Muscle fibers, when isolated from an organism and stimulated artificially, are capable of contracting 50% of their resting length. However, in most animals, the contraction is constrained by the joints to which the muscle is attached, as a result, the strain is typically less than 20%. Muscle, unlike most artificial muscles, contains sufficient ATP for tens of contraction/relaxation cycles.

There are three types of muscle tissues: skeletal, cardiac, and smooth. Skeletal muscles account for almost 40% of body mass and are the only type of muscle that can be controlled voluntarily. The heart is a pump consisting of specialized cardiac muscle fibers. Smooth muscle tissue is often found in the walls of hollow internal organs (e.g., intestine, stomach, respiratory passages, and urinary bladder) and is responsible for passage of fluids and other substances through the internal body channels by slow and sustained involuntary contractions. Muscles can only actively contract and because they cannot actively expand, they require either an antagonist muscle contraction or a stretched tendon (passive spring) to exert a lengthening force. The muscles found in mammals, most fish, and birds always consume energy to generate and maintain force. An exception to this is found in mollusks where the muscle for controlling the shell closure can go into a catch-state (lock-up state) where it continues to maintain the force holding the shell closed without any further energy consumption. Aside from contracting and performing work, stabilizing joints, maintaining body posture, and generating heat (when contracting) are muscles' other functions.

Until relatively recently, the primary actuator responsible for mobility on the planet was muscle. The skeletal muscles in humans, horses, elephants, oxen, and other mammals generate maximum forces of around 350 kN m^{-2} . However, in different species, the muscle performance varies. Table 1 includes more performance metrics for muscles in different organisms.

3. Artificial Muscles: Working Mechanism, Properties, and Limitations

Artificial muscles or actuators actively contract and/or actively expand in length when excited by a stimulus such as an electric/magnetic field, thermal energy (via phase change or thermal expansion of the active material), electrochemical energy (via Faradaic reaction or charge accumulation in the double layer),



Seyed M. Mirvakili received his BASc degree in electrical engineering with minor in nanotechnology and microsystems from UBC in 2011. For his MSc degree, he joined Molecular Mechatronics Lab in the electrical engineering department at UBC where he finished his degree in 2013. He started his Ph.D. in BioInstrumentation

lab in the mechanical engineering department at MIT in September 2014 and finished his degree in May 2017. He is now a postdoctoral associate in Langer Lab at MIT. He has initiated and worked on various projects on topics including analog circuit design, bio-photovoltaics, energy-storage devices, and artificial muscles for the past decade.



Ian W. Hunter received his B.Sc., M.Sc., and Ph.D. degrees at the University of Auckland, in Auckland, New Zealand in 1974, 1975, 1976, and 1980, respectively. He was affiliated with the McGill University in Montreal, Canada from 1980 until 1994 when he joined the faculty of MIT in Cambridge, Massachusetts where he

presently is the Hatsopoulos Professor of Mechanical Engineering and head of the BioInstrumentation Laboratory. His current research interests are microinstrumentation, microfabrication, microrobotics, microsurgical robotics, artificial-muscle fibers, laser-imaging systems, instrumentation physics, and conducting-polymer energy storage and actuators.

fluid pressure (in the form of pneumatic or swelling pressure), and light.^[1] An early example of a non-muscle-based actuator dates back to early civilizations (e.g., Mesopotamia and ancient Egypt) where metallic wedges were inserted into cracks of rocks and heated with fire to split them via the thermal expansion in the wedge. For thousands of years, biological muscle was the major driving force for performing work. For example, battles were originally largely fought using muscle welded weapons (swords, bows, clubs, etc.).

With the development of explosive gunpowder in the 1400s, much higher force and power densities became available. In the 1670s, the Dutch mathematician and scientist Christian Huygens invented a linear actuator in which the explosion of a charge of gunpowder forced a piston to move inside a cylinder. Huygens calculated that when exploded, 1 pound of gunpowder could raise an object weighing 3000 pounds by 30 feet. This corresponds to a gun powder energy density of 270 kJ kg^{-1} , which is about 10% of that of modern gunpowder formulations.^[5]

Table 1. Biological muscle.

Property	Typical	Maximum
Strain [%] ^[4]	20	>40
Stress [MPa]		
Mammals (e.g., human) ^[4]	0.1 (sustainable)	0.35
Aquatics (e.g., mollusks)	–	≈1
Work density [kJ m ⁻³] ^[4]	8	40
Density [kg m ⁻³] ^[4]	1037	–
Strain rate [% s ⁻¹] ^[4]	–	>50
Specific power [W kg ⁻¹]		
Human ^[4]	50	284
Chameleon (tongue) ^[6]	–	14 000 ^{a)}
Bumblebee	–	350
Hummingbird ^[7]	75	309
Moth ^[8]	35	90
Cockroach	6.5 ^[8]	19–25 ^[9]
Fish ^[11]	6	28
Froghopper ^[12,13]	36 000 ^{a)}	74 000 ^{a)}
Planthopper ^[14]	37 600 ^{a)}	160 300 ^{a)}
Bandwidth [Hz]		
Human	–	20
Midges ^[15]	–	1000
Efficiency [%] ^[4]	–	40
Cycle life ^[4]	–	>10 ⁹
Modulus [MPa] ^[4]	10–60	–

^{a)}Note that it is not solely due to the muscle activation: some fraction of energy is stored as elastic energy and is released in a very short period of time. The maximum power a muscle can produce is typically between 100 and 500 W kg⁻¹ in all animals.

One of the earliest references to modern artificial muscles can be found in works of the scientist and engineer Robert Hooke. He investigated the physiology of various muscles and in the 1670s, proposed a number of schemes to build artificial muscles including ones actuated using gunpowder. He claimed that he “had a way of making an artificial muscle to command the strength of 20 men.”^[16]

In the following sections, properties, designs, as well as application of different actuators are discussed. Some categories have evolved rapidly over the past decade while others achieved barely noticeable progress. Here, we focus on recent results for each category and older technologies are only briefly mentioned for the sake of completeness. It is important to note that the values we have gathered in the tables for each category are the best numbers that authors have reported in their articles.

3.1. Highly Oriented Semicrystalline Polymer Fibers

Polyethylene and nylon fibers, when highly oriented along their length, exhibit anisotropic thermal expansion behavior.^[17–19] For example, Nylon 6,6 (such as those used in

Table 2. Properties of Nylon-6,6.

Property	Nylon-6,6 ^{a)} ^[19]	
Thermal conductivity [W m ⁻¹ K ⁻¹]	≈0.09 ^{b)}	
Thermal diffusivity [mm ² s ⁻¹]	≈0.11 ^{b)}	
Density [kg m ⁻³]	≈1150 ^{b)}	
Specific heat capacity [J kg ⁻¹ K ⁻¹]	≈1531 ^{b)}	
T _g [°C]	49	
Storage modulus [MPa]	@20 °C	2400
	@150 °C	260
Thermal expansion coefficient [K ⁻¹]	T > T _g	>–2.8 × 10 ^{–4}
	T < T _g	<–2.8 × 10 ^{–5}

^{a)}These data are for Nylon 6,6 precursor that is used in ref. [19]; ^{b)}At room temperature.

high-performance fishing lines and sewing threads) can contract in length by up to 2.5% while expand in diameter by up to 4.5% (more properties in **Table 2**).^[19] This remarkable property has enabled fabrication of linear,^[17,18,20,21] torsional,^[22] and bending^[19] actuators from these inexpensive ($\approx \$5 \text{ kg}^{-1}$) polymer fibers (**Figure 1**). For example, coiled nylon actuators, fabricated through extreme twisting of nylon 6,6 fibers, have demonstrated contractile actuation of up to 49% (Figure 1A,B).^[17]

3.1.1. Working Mechanism

Some thermoresponsive polymers such as nylon have semicrystalline structure. Upon heating, the crystalline regions expand in volume while the amorphous chains shrink in length. The amorphous phases are energetically less stable than the crystalline phases. Therefore, when highly oriented, the fiber shrinks in length while expands in diameter (Figure 1I, inset).^[19,23] The required heat can be supplied via Joule heating, convective heating, or photothermal excitation. In Joule heating, current is passed through an electrically resistive material that is coated on the surface of the filaments. The resistive coatings that are demonstrated so far are multiwalled carbon nanotube (MWCNT) yarns,^[17] silver plated coating,^[17] silver paint,^[18] silver–niobium nanowire (NW) paint,^[19] and nichrome wire.^[24,25] Unlike in Joule heating, in convective heating, the surrounding medium is responsible for providing the heat. For example, hot/cold air or liquid such as water transfers the heat to the filaments (Figure 1G,H).^[17] In photothermal excitation, absorption of light at the surface of the actuator creates the required heat for actuation. For this type of excitation, surface coatings with high light-absorption coefficient are ideal. Graphene coating, due to the color and high thermal conductivity of graphene particles, has shown to work well in excitation with high power laser diodes.^[19] **Table 3** contains the results obtained for linear artificial muscles from these highly oriented semicrystalline polymer fibers.

Twisted-coil nylon fibers are shown to produce torsional stroke when differentially heated with hot air along their length (more on the mechanism in “Twisted Nano-/Microfiber Yarns” Section) for application in energy harvesting from waste heat

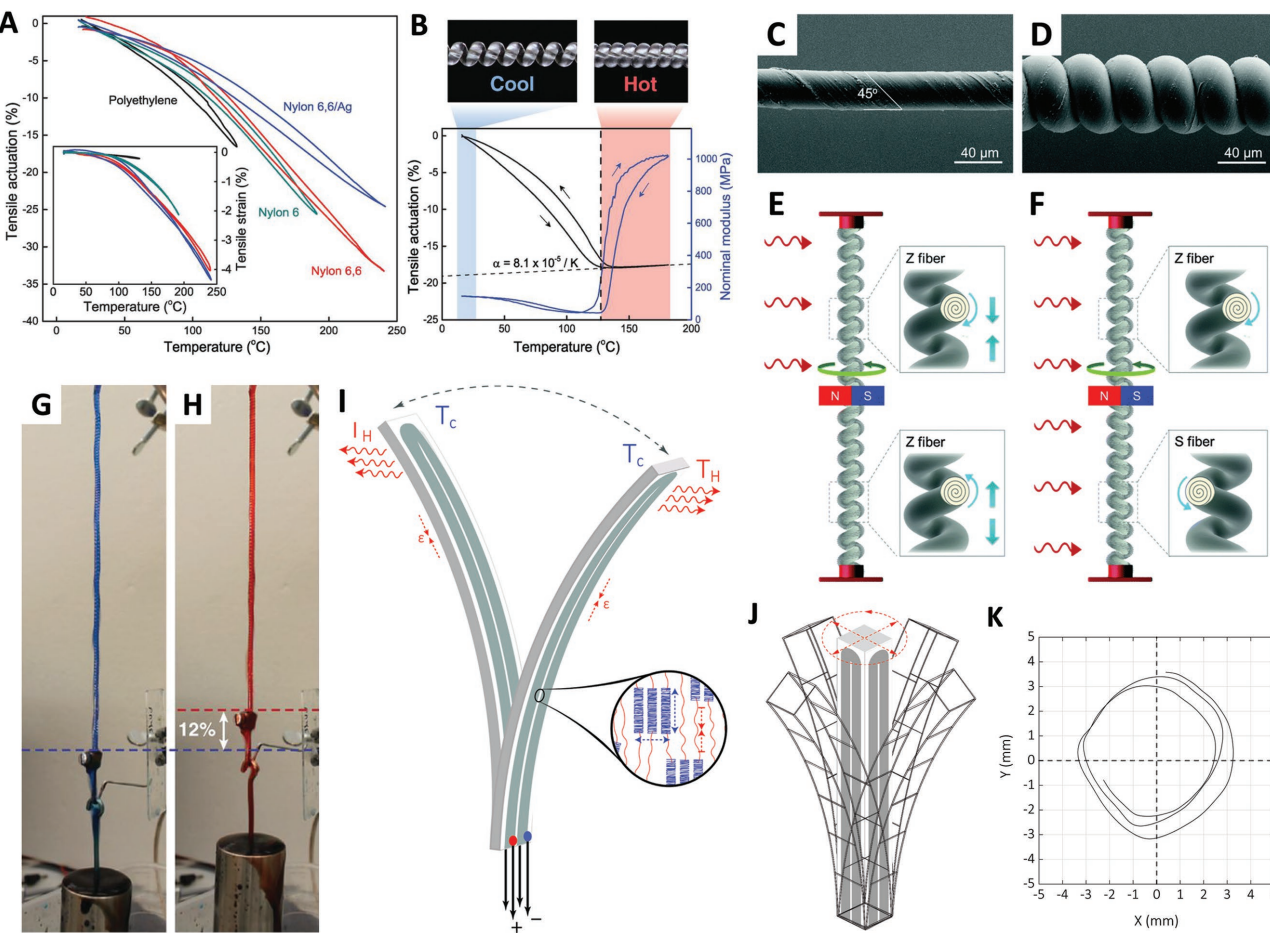


Figure 1. A) Comparison of the negative thermal expansion of braided polyethylene, nylon-6 monofilament, nylon-6,6 monofilament, and silver-coated nylon-6,6 multifilament fibers before twisting (inset) and after coiling by twist insertion. B) Tensile stroke and nominal modulus versus temperature for a coiled, 300 μm diameter nylon-6,6 monofilament muscle under 7.5 MPa static and 0.5 MPa dynamic load. During contraction, neighboring coils come into complete contact at ≈ 130 $^{\circ}\text{C}$, which dramatically increases the nominal elastic modulus and causes the thermal-expansion coefficient to become positive. Optical microscopy images (top) of the coils are shown before and after contact. C–F) Torsional artificial muscle from nylon used to harvest heat. (C) Twisted muscle fiber prepared by inserting 8350 turns m^{-1} of twist into a 27 μm diameter nylon-6,6 fiber to provide a bias angle of 45°. (D) Coiled muscle fiber prepared by inserting an additional 2850 turns m^{-1} of twist into the above twisted fiber. The outer diameter of the nonloaded coil is 62 μm and its spring index is 1.14. (E) The homochiral ZZ fiber configuration used for torsional energy harvesting. The top half of the coiled fiber untwists during heating and contracts, while the unheated bottom half serves as a return spring by up-twisting and stretching. (F) The heterochiral SZ fiber configuration used for torsional energy harvesting. When fully heated, the coiled S fiber and coiled Z fiber simultaneously untwist to provide the same direction torque on the rotor. Red fiber-end attachments prohibit both rotation and translation. G,H) Hydrothermal actuation of a coiled 860 μm diameter nylon-6 fishing line lifting a 500 g load by 12% when switched at 0.2 Hz between ≈ 25 $^{\circ}\text{C}$ water (dyed blue) (G) and 95 $^{\circ}\text{C}$ water (dyed red) (H). I–K) Multidirectional artificial muscle from highly oriented nylon: (I) By heating one side of the actuator, the amorphous chains (red lines) shrink in length and the crystalline regions (blue lines) expand in volume. The result is surface contraction of the beam at its heated surface which creates the bending motion. (J) Schematic of the multidirectional actuator. (K) The coordinate of the tip of the actuator by applying the following input voltages to different sides of the actuator (left to right): X-Ch: $V_x = V_{x0}\sin(\omega t)$, Y-Ch: $V_y = V_{y0}\cos(\omega t)$. (A,B,G,H) Reproduced with permission.^[17] Copyright 2014, American Association for the Advancement of Science. (C–F) Reproduced with permission.^[22] Copyright 2015, Royal Society of Chemistry. (I–K) Reproduced with permission.^[19] Copyright 2017, Wiley-VCH.

(Figure 1C–F).^[22] Table 4 includes the results obtained for these actuators.

Aside from linear and torsional actuators, multidirectional actuators are also demonstrated from nylon 6,6 filaments.^[19] It is shown that by changing the cross-sectional area of nylon filaments from circle to rectangle or square and differentially heating the sides, the actuator can bend in 1D or 2D, respectively (Figure 1I–K).^[19] Although thermal actuators have small bandwidth (on the order of several hertz), high actuation frequencies

(at the resonance) are demonstrated.^[19] This can be achieved by adjusting the dimensions of the beam and tuning the natural frequency (ω_n) according to the following equation^[19]

$$\omega_n \sim \frac{t}{L^2} \sqrt{\frac{E}{\rho}} \quad (1)$$

where t is the thickness, L is the length, E is the Young's modulus, and ρ is the volumetric mass density of the actuator.^[19]

Table 3. Linear artificial muscle from highly oriented semicrystalline polymer fibers.^[17]

Property	Nylon-6,6	Nylon-6	Nylon-6,6 (silver plated)	Polyethylene
Stimulus	Heat	Heat	Heat	Heat
Amplitude of stimulus	240 °C	190 °C	240 °C	130 °C
Strain ^{a)} [%]	4 (@15 MPa) 33 (@15 MPa)	2.2 (@3.5 MPa) 49 (@1 MPa)	4.4 (@7.8 MPa) 24 (@15 MPa)	0.2 (@15 MPa) 16 (@15 MPa)
Stress [MPa]	22 (@10%)	8.4 (@12%)	38 (@10%)	–
Work density	2.48 kJ kg ⁻¹ (84 MPa)	–	–	2.63 kJ kg ⁻¹ (@140 MPa)
Specific power [kW kg ⁻¹]	27.1	–	–	5.26
Bandwidth [Hz]	7.5 (in helium)	–	5 (in water)	2 (in water)
Efficiency [%]	<1	<1	<1	<1
Cycle life	1.2 × 10 ⁶ @10%	–	–	–

^{a)}All results here are for twisted-coiled artificial muscles except the first row of the strain results.

Table 5 shows the results achieved for bending artificial muscles made of nylon fibers.

3.1.2. Limitations

One of the common rate limiting factors in thermal actuators is the heat transfer rate during actuation and relaxation. Submerging the actuator in a coolant such as water or ethanol have shown to increase the cycling rate,^[17,18] but still the bandwidth is smaller than that of most other actuators.

During the thermal excitation, heat transfers from the outer surface of the filament to the inner part via conduction. The time constant for the heat diffusion is

$$\tau \sim \frac{t^2}{4\alpha} = \frac{\rho t^2 C_p}{4k} \quad (2)$$

where t is the thickness, α is the thermal diffusivity, ρ is the volumetric mass density, C_p is the specific heat capacity, and k is the thermal conductivity. During cooling in air, convective heat transfer is the dominant process and has the time constant of

$$\tau = \rho C_p \frac{t}{h} \quad (3)$$

Table 4. Torsional artificial muscles from nylon fibers.

Property	Nylon-6, ^[17]	Nylon-6, ^[22]	Nylon-6, ^[17]
Stimulus	Joule heat	Heat	Heat
Geometry	Straight	Coiled	Straight
Amplitude of stimulus	140 mW cm ⁻¹	ΔT = 62 °C	160 °C
Torsional stroke [° mm ⁻¹]	<5.5	<210	<7
Torsional speed [rpm]	<70	<70 000	–
Torque [N m kg ⁻¹]	–	0.8	–
Peak work density	–	0.3 mJ m ⁻¹	2 kJ kg ⁻¹ (@14 mN m)
Specific power [W kg ⁻¹]	–	1900	–
Cycle life	–	10 ⁵	–

where ρ is the volumetric mass density, t is the thickness, C_p is the specific heat capacity, and h is the heat transfer coefficient of free air convection at the boundary.

As Equations (2) and (3) suggest, thickness and heat transfer coefficient play an important role in determining the bandwidth. We can expect in the future that incorporation of very high thermally conductive materials such as graphene ($k = 2000 \text{ W m}^{-1} \text{ K}^{-1}$) can result in both faster actuation in thermal actuators, thus increasing peak power density, and prolonged higher force generation in Lorentz force actuators, hence increasing the energy density. As fabrication techniques allow for greater level feature size miniaturization, diffusion distances for heat or mass (e.g., ion, molecule) transport decrease with corresponding increased performance via Equations (2) and (3). For example, the thermal actuators in inkjet printers head have become faster (sub-millisecond) as fabrication techniques have created finer structures.

3.1.3. Applications

Smart windows, energy-harvesting systems, linear actuator for locks, smart fabrics, and actuators for robotic exoskeletons, and arms are some envisioned applications for these actuators.

Table 5. Bending artificial muscle from nylon fibers.

Property	Nylon-6, ^[19]
Stimulus	Heat
Amplitude of stimulus	ΔT = 65 °C
Bending amplitude ^{a)}	1.25
Blocking force ^{b)} [MPa]	55
Catch-state	Yes
First resonance frequency ^{c)} [Hz]	17
Efficiency [%]	<1
Cycle life	10 ⁵

^{a)}Peak-to-peak amplitude normalized to the length of the actuator; ^{b)}Blocking force normalized by the dimensions as described in ref. [19]; ^{c)}Dimension dependent.

3.2. Nanoparticle-Based Actuators

Thanks to the advances in the field of nanotechnology, many new carbon-based nanoparticles and porous polymer films are discovered and synthesized, enabling fabrication of micro-/nanostructures for actuators and energy-storage devices.

Carbon nanotubes, graphene, and fullerenes, in particular, have attracted attentions in the field of artificial muscles owing to their excellent porosity and good electrical conductivity. Linear and bending actuators are demonstrated from pure carbon nanoparticles and/or their composites with polymers, hydrogels, or other nanomaterials (Figure 2).

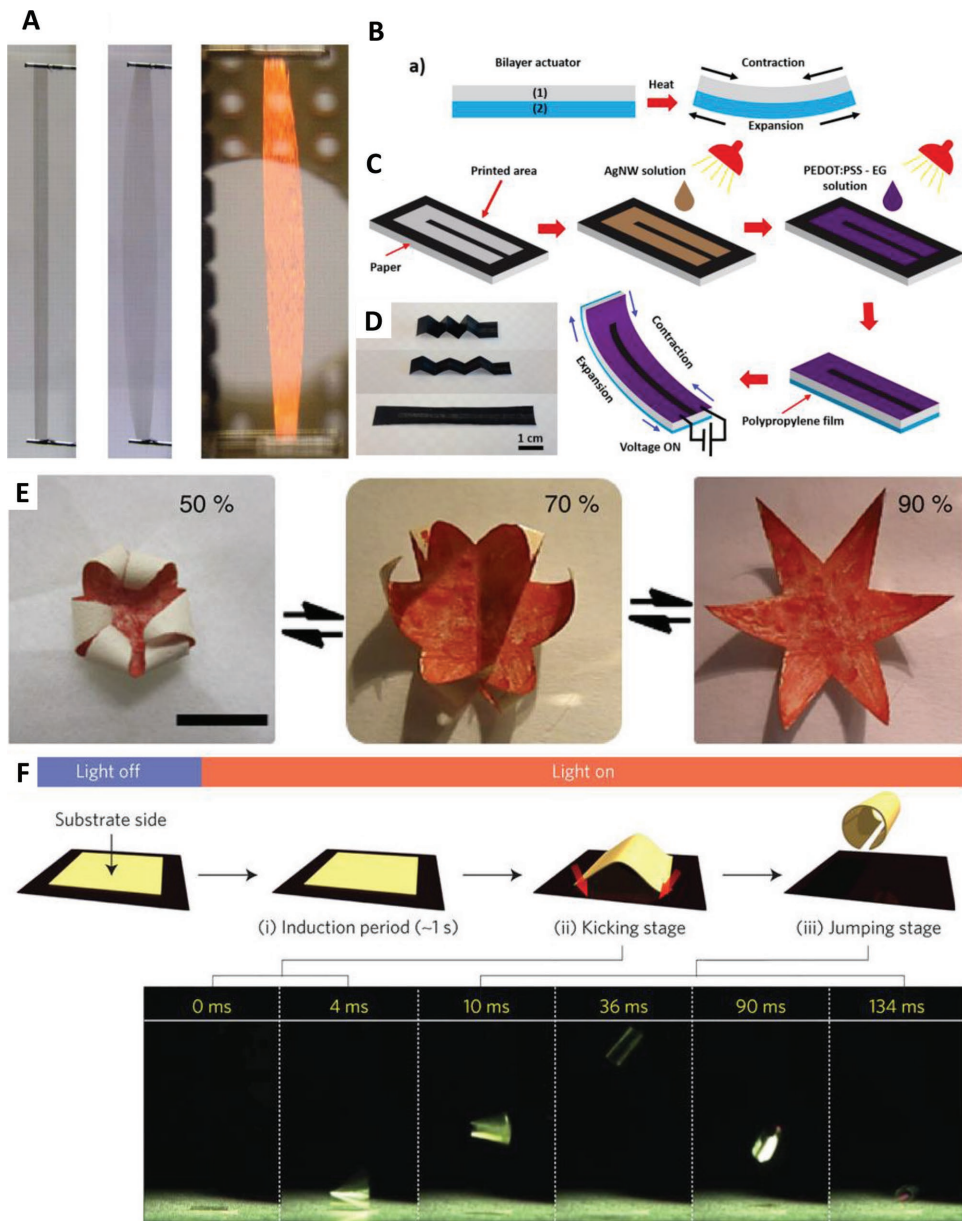


Figure 2. A) Left and middle: Photograph of a rigidly end-supported 50 mm long by 2 mm wide nanotube-sheet strip (left) and the same sheet strip expanded in width by applying 5 kV with respect to ground (middle). Right: Photograph of a 25 mm long nanotube-sheet strip actuated at 1500 K by applying 3 kV, where the color of incandescence is not correctly captured by the camera. B) Schematic illustration of a bilayer structure composed of two active layers. C) Fabrication process of the paper-based actuators. D) Optical images of a patterned hybrid film on the paper substrate before and after folding. E) The reversible closing and opening of a star-shaped membrane actuator "flower" upon switching the humidity between 50% and 90% at 20 °C; here, the top surface of the membrane was stained red, while the bottom surface retains the original light-yellow color; the inserted number is the relative humidity; scale bar: 1 cm. F) Schematic representation and high-speed snapshots of the jumping motion of a carbon nitride polymer (CNP) film on exposure to ultraviolet light. All of the films were obtained by vapor-deposition polymerization (VDP) onto a glass substrate and then peeling off. (A) Reproduced with permission.^[26] Copyright 2009, American Association for the Advancement of Science. (B–D) Reproduced with permission.^[27] Copyright 2016, American Chemical Society. (E) Reproduced with permission.^[28] Copyright 2014, Macmillan Publishers Limited. (F) Reproduced with permission.^[29] Copyright 2016, Macmillan Publishers Limited, part of Springer Nature.

3.2.1. Stimuli

Thermal energy from light absorption^[30–32] or Joule heating,^[33,34] charge injection in the double layer,^[35] and humidity/solvent molecule sorption^[28,29,36–39] are among the common stimuli that are investigated so far according to the literature.

3.2.2. Mechanism

The actuation mechanism in nanoparticle-based films as well as porous polymer films depends on the stimulus. In guest-infiltrated films, thermal expansion of the guest material, such as paraffin wax,^[40] is responsible for the volumetric expansion of the film, while in electrochemically activated films (usually exhibiting high specific electric double layer (EDL) capacitance), charge accumulation in the double layer is the key working mechanism. In humidity/solvent molecule sorption, the pressure induced by swelling creates the required stress for actuation in the film.^[28,29,36–39] However, in composite films that are activated with light, carbon nanoparticles (e.g., single-walled carbon nanotubes or graphene) absorb the light and efficiently transfer the generated heat to an underlying thermally responsive polymer or hydrogel film.^[19,30–32] In Joule heating, actuator nanomaterials are utilized because of their negative thermal expansion coefficient (e.g., graphene or carbon nanotubes with particular alignments),^[33,34,41–43] and/or their good resistivity which makes them suitable as a resistive heating element.^[19,27,43,44] It is important to note that in thermally activated bending actuators, the key driving force is the difference between thermal expansion coefficients on the opposite surfaces of the film (i.e., $\alpha_{\text{top}} - \alpha_{\text{bottom}} \neq 0$).^[45] Therefore, coatings that can significantly modify the thermal expansion coefficient of the actuator's structure are desirable. In general, any asymmetric response from the surfaces of an actuator to an external stimulus can generate bending-type actuation in films or beams.

The generated strain from nanoparticle films is typically small (<2%), which is mostly due to the physical properties of these materials (e.g., low thermal expansion coefficient, high elastic modulus) (Table 6). Giant strokes up to 220% (along

Table 6. Nanoparticle-based actuators.

Property	Nanoparticle-based
Strain [%]	1.5, 220 ^{a)} [26]
Stress [MPa]	115 ^[36]
Strain rate [% s ⁻¹]	3.7 × 10 ⁴ [26]
Response time [s]	0.3 ^[36]
Work density [J kg ⁻¹]	40 ^[41]
Power density [W kg ⁻¹]	3.2 ^[41]
Tensile strength [MPa]	<500 ^[36]
Bandwidth [Hz]	0.5 ^[33,35] (first resonance at ≈100 Hz) ^[35]
Efficiency [%]	0.01% ^[32]
Cycle life	60 000 ^[32]

^{a)}Measured along the length and width, respectively.

the width of the muscle) are achieved from multiwalled carbon nanotube aerogel muscles at extreme excitation conditions (3 kV @1500 K) but with only <1.5% actuation along the length of the muscle (Figure 2A).^[26] To amplify this small strain, these materials are typically utilized in a bimorph structure (Figure 2B–F). Equation (4) shows the relationship between the curvature (κ) (measured from the surface of the actuator) and the strain at the surface of the film (ϵ)^[19]

$$\kappa = R^{-1} = \frac{2}{t} \frac{\epsilon}{1 - \epsilon} \quad (4)$$

where R is the radius of curvature (measured to the surface of the actuator) and t is the thickness of the film, respectively. Measuring the radius of curvature to the middle of the actuator's thickness leads to curvature of $2\epsilon/t$. The strain at the surface of the film (ϵ) can be estimated from the peak displacement amplitude at the tip (A) (which is half of the full dynamic range for a bidirectional bending actuators), length (L), and thickness (t) of an actuator as follows^[19]

$$\epsilon = \frac{tA}{A^2 + L^2} \quad (5)$$

The strain difference between the top and bottom surfaces is double the strain given by Equation (5) (derivation of Equations (4) and (5) can be found in the Supporting Information of ref. [19]).

3.2.3. Limitations

The limitations for this category of actuators are mostly dependent on the stimulus. For example, for heat-activated actuators, the efficiency is typically low and the cooling time constant is a rate limiting factor, while for electrochemical actuators, the ionic conductivity of the electrolyte as well as the specific capacitance of the structure defines the actuation speed (more on this in the section on conducting-polymer actuators). The performance of actuators activated by moisture and molecule sorption is very much dependent on the size of the molecule as well as the migration rate. Aside from all the mentioned limitations, cycle life and cost play key roles if commercialization of these actuators is desired.

It is important to note that although individual sheets of graphene and carbon nanotubes have remarkable electrical and mechanical properties, in bulk, due to the weak interactions between the individual components, those properties are not exceptional any more. Table 6 contains the results for nanoparticle-based actuators.

3.2.4. Applications

Some envisioned applications for nanoparticle-based actuators are humidity sensors,^[29,39] light-intensity sensors,^[31] morphing microrobots, micro-electromechanical systems (MEMS), smart

curtains,^[32] moisture-responsive air flow valves, robotic grippers,^[33] and many more.

3.3. Twisted Nano-/Microfiber Yarns

Twisted yarns of nano-/microfibers (e.g., multiwalled carbon nanotube, nanowire, graphene) can generate linear and torsional actuation upon volumetric expansion of the yarn. One interesting example of a material with such a property is hair. Until fairly recently, a common way to actuate the dial of a humidity sensor was to use the hydroscopic dependence of the length of an animal hair (e.g., from a horse tail) on its water content. The first such hair hydrometers date back to the mid-1600s.

Volumetric expansion in the twisted nanofiber yarns can be achieved via different mechanisms including volumetric thermal expansion of a guest material (Figure 3A–K),^[46–48] volumetric expansion of a guest material due to physical absorption (Figure 3P),^[49] and charge injection in the double layer (Figure 3M–O).^[50,51] Torsional actuation can be obtained from the shape-memory effect as well. More details on this are discussed in the section on thermally activated shape-memory alloys (Figure 3L).

3.3.1. Working Mechanism

A one-end-tethered twisted yarn responds to any structural volumetric change by untwisting at its free end. This behavior can

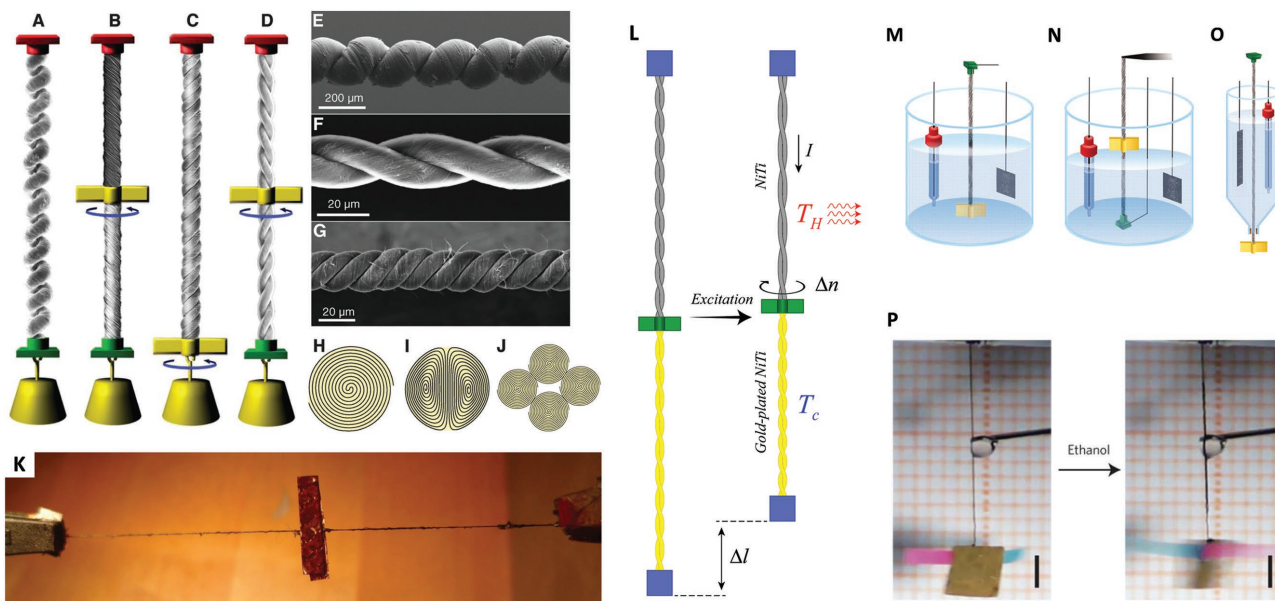


Figure 3. A–J) Muscle configurations and yarn structures for tensile and torsional actuation. Tensile load and paddle positions for a two-end-tethered, fully infiltrated homochiral yarn (A); a two-end-tethered, bottom-half-infiltrated homochiral yarn (B); a one-end-tethered, fully infiltrated homochiral yarn (C); and a two-end-tethered, fully infiltrated heterochiral yarn (D). The depicted yarns are coiled, noncoiled, four-ply, and two-ply, respectively. The arrows indicate the observed direction of paddle rotation during thermal actuation. The red and green yarn-end attachments are tethers, meaning that they prohibit end rotation; the red attachments also prohibit translational displacement. Scanning electron microscopy (SEM) images of a fully infiltrated homochiral coiled yarn (E), a neat two-ply yarn (F), and a neat four-ply yarn (G). Illustration of ideal cross-sections for Fermat (H), dual-Archimedean (I), and infiltrated four-ply Fermat (J) yarns. K) Torsional artificial muscle from niobium-nanowire yarn. The right half of the yarn is infiltrated with wax and melting induced by current pulses creates the torsional actuation. The central paddle is used to determine rotation. It has a mass 23 times larger than the yarn's and a moment of inertia of $3.3 \times 10^{-10} \text{ kg m}^2$. The yarn is held at constant length. The yarn diameter without wax is 51 μm , the inserted twist is 2381 turns m^{-1} , the distance between clips is 6.3 cm, and the paddle is 13 mm long by 3 mm wide. L) Diagram illustrating the working mechanism of a shape-memory-alloy-based torsional actuator. The bottom yellow part of the yarn represents the gold-coated section. M–O) Illustration of electrochemical-cell configurations used for characterizing torsional actuation or the combination of torsional and tensile actuation, where the Ag/Ag⁺ reference electrode, actuating MWCNT yarn electrode, and Pt mesh counter electrode are shown from left to right: a one-end-tethered yarn configuration in which a paddle, located at the yarn end, rotates in the electrolyte (M); a two-end-tethered configuration for simultaneously measuring torsional and tensile actuation, in which the top yarn support is a force–distance transducer that maintains constant tensile force on the yarn and measures the axial length change as the paddle rotates in air (in other cases, the electrolyte level was raised to submerge the paddle) (N); a one-end-tethered configuration in which the paddle rotates in air (O). P) Photographs of ethanol diffusion along a hierarchically arranged helical fiber (HHF) before the formation of coils. Left image: the fiber at the instant of coming into contact with an ethanol droplet (the hanging yellow copper paddle was stationary). Right image: the fiber at 1.63 s after coming into contact with ethanol (a rotary actuation was generated during ethanol diffusion along the fiber). The pink and blue paper slips were fixed on the copper paddle to record the revolution using background coordinate paper. Scale bars: 2 mm. (A–J) Reproduced with permission.^[46] Copyright 2012, American Association for the Advancement of Science. (K) Reproduced with permission.^[47] Copyright 2013, Wiley-VCH. (L) Reproduced with permission.^[52] Copyright 2017, American Chemical Society. (M–O) Reproduced with permission.^[50] Copyright 2011, American Association for the Advancement of Science. (P) Reproduced with permission.^[53] Copyright 2015, Macmillan Publishers Limited (Springer Nature).

be explained from the helix geometry.^[46,47,52] In a one-end-tethered twisted yarn, assuming the fibers are inextensible, the only way that the helical structure can accommodate any changes in its diameter is to untwist. Now, if two ends of the yarn are tethered, the change in diameter translates into contraction in length only. For the special case of having only half of a two-end-tethered yarn infiltrated with a guest material, the infiltrated section of the yarn untwists, while the bare part twists and acts as a bias torsional spring. For a twisted yarn with individual fiber length of L , yarn length of h , diameter of d , and twist angle of α (the angle between the fibers and the yarn axis), the torsional stroke (i.e., $\Delta N/N$) can be described by the helix geometry as the following equation suggests^[52]

$$\frac{\Delta N}{N} = \frac{\Delta L}{L \sin^2(\alpha)} - \frac{\Delta h}{h \tan^2(\alpha)} - \frac{\Delta d}{d} \quad (6)$$

Helix geometry does not contain any information on the number of twists in each individual fiber and its contribution to the torsional stroke during excitation. A more complete model can be derived from spring mechanics to include the contribution of the number of twists in each individual fiber (i.e., n).^[52] The following equation describes the torsional stroke in terms of the tensile strain in each individual fiber, tensile strain of the yarn, strain in radial direction, and torsional stroke of each individual fiber ($\Delta n/n$)^[52]

$$\frac{\Delta N}{N} = 3 \frac{\Delta L}{L} - \frac{\Delta h}{h} - \frac{1}{2} \frac{\Delta d}{d} + \frac{\Delta n}{n} \quad (7)$$

Torsional stroke of each individual fiber is very important for the cases that each fiber can untwist during excitation (refer to the section on thermally activated shape-memory alloy fibers, for examples).

3.3.2. Stimuli

Any stimulus that can create a volumetric expansion can be used to actuate twisted nanofiber yarns. Twisted nanofiber yarns basically convert one form of actuation (i.e., volumetric expansion) to another (i.e., linear and torsional). The actuation mechanisms that are explored so far are:

Thermal Excitation: One of the chemicals with an extraordinary thermal expansion coefficient is paraffin wax. During phase transition, paraffin wax expands in volume by 30%.^[46] By infiltrating twisted nanofiber yarns with paraffin wax and heating the yarn (via Joule heating, for example), tensile and torsional actuation can be achieved.^[46–48]

Charge Injection in Double Layer: Electrical double layer forms at the electrolyte–electrode interface when a voltage is applied to the conductive electrodes. The thickness of the double layer, which is on the order of one to few tens of nanometers, can be estimated from the Debye length (κ^{-1}), which is inversely proportional to the square-root of the molar concentration of the electrolyte. Electric double layer creates repulsive forces

between the charged surfaces, which act over distances that are comparable to the Debye length.^[54] Therefore, in twisted porous yarns – such as multiwalled carbon nanotube yarns – formation of the double layer leads to an increase in the diameter of the yarn which translates to torsional and linear actuation as described above.^[50,51,55]

Swelling Pressure: Absorption of solvents can lead to volumetric expansion in some materials. For example, yarns of cotton or cellulosic nanofibers (such as the cellulose fibrils in wheat awns) swell water, while rubber swells organic solvents. Volumetric swelling can be up to 400% in some cross-linked elastomers, which is much larger than the 30% volumetric thermal expansion of paraffin wax.^[49] Infiltrating nanofiber yarns such as multiwalled carbon nanotube yarns with solvent-responsive compounds have demonstrated torsional and linear actuation.^[49,53,56–60]

Similar to hair, spider dragline silk is another example of microfiber actuators made by nature. Spider dragline silk undergoes large expansion in its diameter when it absorbs moisture. These fibers are semicrystalline structures which are made of highly oriented crystalline β -sheets and amorphous polypeptide chains and helical structures.^[61] At high humidity, the dragline silk supercontracts (50% strain under no load, 50 MPa stress under blocking force test) due to the disruption of the hydrogen bonds within the amorphous regions of the fiber.^[62] This modification in the hydrogen bonds increases the molecular mobility, which drives the proteins into a less organized configuration, leading to supercontraction.^[62] The supercontraction occurs only once but humidity fluctuation can still generate small values of strain in the dragline silk fiber.^[62] Table 7 shows the results for twisted nano-/microfiber-based artificial muscles.

3.4. Thermally Activated Shape-Memory Alloy (SMA)

Shape-memory alloys, a member of the shape-memory material family, can retain their original form (shape or size) upon excitation with a stimulus such as heat. For example, a bent or twisted shape-memory alloy wire recovers its original shape (i.e., unbent or untwisted) when excited with heat. This remarkable property has made SMAs very popular in research and development since their discovery in 1932 by Arne Ölander.^[63] The field of shape-memory alloys is very broad and extensively studied and have branches in material design, device design, and control system design. In this section, we focus only on linear, torsional, and bending artificial muscles made of SMA materials.

Alloys of nickel–titanium (e.g., NiTi, NiTiCu, NiTiFe, etc.), iron (e.g., FePt, FeNiC, etc.), copper (e.g., CuSn, CuZn, etc.), silver (e.g., AgCd, etc.), gold (e.g., AuCd, etc.), and cobalt (e.g., CoNiAl, etc.) are examples of shape-memory alloy metals that are commercially available. Nickel–titanium (NiTi) – one of the most popular and well-studied SMA metals^[64,65] – outperforms most of the other SMA metals such as iron or copper-based alloys in terms of mechanical and thermomechanical properties.^[66] The shape-memory effect in NiTi alloy was discovered in the 1960s in the Naval Ordnance Laboratory where the term “nitinol” was coined for this alloy to note the name of its composition and place of discovery.^[67,68]

Table 7. Twisted nano-/microfiber-based torsional and linear actuators.

Property	MWCNT	MWCNT-coiled	MWCNT/wax-coiled	Niobium NW/wax	MWCNT	MWCNT/rubber	Spider-silk dragline
Stimulus	EDL ^[50]	EDL ^[51]	Heat ^[46]	Heat ^[47]	Ethanol absorption ^[53]	Organic solvent absorption ^[49]	Water moisture absorption ^[62]
Amplitude of stimulus	2 V ^{a)}	3.25 V ^{a)}	80–210 °C	80–210 °C	Dry to wet	Dry to wet	Relative humidity (RH) 10–90%
Strain [%] ^{b)}	1 (@88 MPa)	16.5 (@25 MPa)	9.5 (@5.5 MPa)	0.24 (@20 MPa)	<65 (@no load)	50 (@2 MPa)	2.5
Stress [MPa]	88 (@1%)	60 (@4.5%)	84 (@3.3%)	20 (@0.24%)	1.5	45	80
Work density	1.1 kJ kg ⁻¹	2.2 kJ kg ⁻¹	1.36 kJ kg ⁻¹ (@84 MPa)	48 kJ m ⁻³	–	1.2 kJ kg ⁻¹	500 kJ m ⁻³ (@53 MPa)
Specific linear power [W kg ⁻¹]	920	<15	27 900	<10	–	4400	130–190
Strain rate [% s ⁻¹]	1	<<1	120	<1	–	80	<1
Torsional stroke [° mm ⁻¹]	250	–	16	12	738	–	–
Torsional speed [rpm]	<590	–	<11 500	<7200	<6500	–	–
Torque [N m kg ⁻¹]	1.85	–	8.2	0.9	–	–	–
Specific torsional power	61	–	–	35	–	–	–
Bandwidth [Hz] ^{c)}	1 (tested) ^{d)}	0.5	20 (tested)	<5	–	1	<<1
Efficiency [%]	<10	5.4	< 2	<2	–	4.3	–
Cycle life	<5000	3000 @3%	1.4 × 10 ⁶ @3%	–	50	1600 @2%	–

^{a)}With respect to an Ag/Ag⁺ reference electrode; ^{b)}The strain values are the maximum numbers that are reported at the mentioned stress value; ^{c)}The bandwidth is the 3 dB bandwidth (the cut-off frequency is at which the amplitude becomes half); ^{d)}The bandwidth depends on the size of the RC time constant of the actuator which is function of the ionic conductivity of the electrolyte and capacitance of the immersed yarn.

3.4.1. Mechanism

Shape-memory alloys often can transform reversibly between two phases (i.e., martensite and austenite), exhibiting three crystal structures (i.e., twinned martensite, detwinned martensite, and austenite). Upon excitation with heat, phase transformation from martensite to austenite starts at temperature A_s and stops at temperature A_f . In this process, a nitinol wire can contract up to 4.5% in length with Poisson's ratio of 0.33.^[52] During cooling, the reverse phase transformation (i.e., austenite to martensite) starts at temperature M_s and stops at temperature M_f . The upper limit temperature at which the martensite reaches its threshold for the applied stress is M_d .^[69] Above M_d , the SMA deforms permanently like any other metals but below that and above A_f , due to twinning, martensite formation under stress allows pseudoelasticity or superelasticity.^[70]

By adjusting the fabrication conditions, the shape-memory effect and the phase transition temperatures can be engineered. The three major shape-memory characteristics for SMAs include one-way shape-memory effect, two-way or revisable shape-memory effect, and pseudo-/superelasticity. In one-way SMAs, the material retains its deformed state after removal of the external stress and recovers its original form after excitation. However, in two-way SMAs, the material can remember its original form at both high and low temperatures. In pseudo-/superelasticity, the material can recover its original form by an external mechanical stress at temperatures between A_f and M_d without requiring thermal excitation.^[71]

Thermal excitation of SMAs can be achieved through Joule heating (aka, resistive heating) or heat transfer via convection

or conduction. Thanks to the electrical conductivity of SMAs (e.g., for nitinol, 0.8 and 1 $\mu\Omega$ m for martensite and austenite phases, respectively)^[52] during Joule heating (at low frequencies), the structure heats entirely (unlike nylon actuators – see the section on highly oriented semicrystalline polymer fibers). During the cooling cycle, heat transfers out of the material via conduction and/or convection which is typically slower than the excitation cycle and limits the cycling rate. It is demonstrated that water/ethanol cooling and nucleate boiling drastically enhance the cooling rate, enabling response time of down to milliseconds.^[72] Excitation of SMA fibers with short high current pulses has shown rapid twitch responses of few milliseconds.^[73] The working mechanism can be explained by the skin effect (at high frequencies, the current density on the outer surface of a metal is the largest). This nonuniform current distribution at high frequencies (or very short pulses) excites the outer shell of the SMA fiber while keeping its inner core unexcited, therefore, the inner core acts as a bias spring and brings the outer shell back to its initial length after excitation.^[73]

SMA wires intrinsically (i.e., in a straight form) can contract up to 8% in length (Table 8),^[74] however, strains more than 100% can be achieved with geometries like helix or zigzag but with lower stresses. Different designs for bending actuators are proposed in which SMA wires in the form of straight wire, helix, or zigzag are utilized.^[75–80]

Torsional actuators are fabricated from SMA wires and tubes, enabling high torsional stroke and torque very comparable to those of electric motors. Two different ways of achieving torsional actuation are proposed: (i) torsional actuation based on

Table 8. Thermally activated linear SMA actuators.^[74,84,87,88]

Property	Thermally activated SMAs
Stimulus	Heat (Joule heating)
Amplitude of stimulus	≈4 V (>> 4 V in short pulse excitation)
Strain [%]	<8.5
Stress [MPa]	<700
Strain rate [% s ⁻¹]	<300
Work density [MJ m ⁻³]	<10
Power density [MW m ⁻³]	<30
Tensile strength [MPa]	<1900
Bandwidth [Hz]	<3 (<35 in a bending actuator) ^[80]
Efficiency [%]	<16% ^{a)}
Cycle life	300 (@≈5%) to 10 ⁷ (@≈0.5%)

^{a)}It is demonstrated in ref. [88] that the efficiency is a function of initial strain.

shape recovery of a twisted fiber/tube;^[52,81–84] (ii) torsional actuation based on linear actuation of SMA wires.^[85,86] The second category focuses on the design aspects of rotary actuators and we are not covering it here.

3.4.2. Torsional Actuation Based on Shape Recovery of a Twisted Fiber/Tube

The shape-memory effect can return a twisted fiber to its initial form, which is a twist-free fiber. By bundling nitinol microfibers, passivating half of the yarn's length, and Joule heating the yarn, it is demonstrated that torsional actuation can be achieved (Figure 3L).^[52,82] The working mechanism is based on untwisting of individual fibers due to the shape-memory effect and generating a large torsional actuation as a bundle (Table 9). More on the modeling of this actuator can be found in the section on twisted nano-/microfiber actuators.

3.4.3. Limitations

SMAs exhibit thermal hysteresis in their strain versus temperature characteristic (i.e., the strain path from M_f to M_s does not follow the path from A_s to A_f), which makes controlling of the actuation very difficult. Typical values for this hysteresis is on the order of tens of degree Celsius. Recently SMA wires,

Table 9. Thermally activated torsional SMA actuators.^[52,82]

Property	Thermally activated SMAs
Stimulus	Heat (Joule heating)
Amplitude of stimulus	2–6 V (14 V in short pulse excitation)
Torsional stroke [° mm ⁻¹]	<46
Rotational speed [rpm]	<10 500
Torque [N m kg ⁻¹]	<28.5
Torsional work density [J kg ⁻¹]	<560
Cycle life	5000

comprising ≈56% weight gold, are demonstrated to exhibit hysteresis of as low as 2 °C.^[89] The stress produced by shape-memory alloys is yet unmatched by any material, but the low cycle life and high fabrication cost (\$200–300 kg⁻¹) limit the applications of this remarkable material.

3.4.4. Applications

The remarkable properties of shape-memory alloys have enabled fabrication of different devices and tools in different industries including biomedical, aerospace, automobile, robotics, etc. Some applications are active catheters, stents, braces, active-compression garments,^[90] robotic arms/legs, microgrippers, camera shutters (in astronomy), airplane components (e.g., flaps), car components (e.g., headlight actuators), miniature robotics, and many more.^[65]

3.4.5. Other Shape-Memory Materials

As mentioned previously, shape-memory alloys are only one category of shape-memory materials. Ferromagnetic shape-memory alloys, shape-memory polymers, and shape-memory ceramics are other members of the shape-memory material family.

Ferromagnetic shape-memory alloys (FSMAs) undergo phase change when exposed to magnetic field. The main advantage of FSMAs over the thermally activated SMAs is that there is no rate limiting factor due to cooling. Thus, bandwidths of up to 1 kHz (@5% strain) can be obtained. Maximum strain of 10% is achieved with maximum stress of 9 MPa.^[4] However, they possess some undesirable attributes such as low operating temperature, high stiffness, and brittleness. More on the working mechanism and modeling of FMSAs can be found in ref. [4].

Shape-memory polymers are very extensible compared to shape-memory alloys (up to 800% vs 8%). They are cheap (≈\$20 kg⁻¹), easy to prepare, and more importantly, can be excited with wider range of stimuli such as heat, magnetic field, and light.^[91]

3.5. Ionic-Polymer/Metal Composites (IPMCs)

Ionic-polymer/metal composites, as the name suggests, are typically composed of an ionically conductive membrane sandwiched between two electron-conductive electrodes. The ionically conductive membrane (IP) contains the electrolyte and is typically made of perfluorinated polymers such Nafion and Flemion which contain ionic sulfonate and carboxylate groups.^[92] Sulfonated hydrocarbon polymers and biopolymers such as cellulose derivatives and chitosan are excellent alternatives to perfluorinated polymers due to their ease of fabrication, cost effectiveness, good ionic conductivity, and environmental friendliness.^[93] Traditionally, gold and platinum were electroplated on the IPs to form the compliant metal contacts.^[94] Thanks to the recent discoveries and advances in the field of nanomaterials, it is shown that carbon-nanotube- and graphene-based electrodes can have some advantages, such as better flexibility and durability, over the conventional noble metal electrodes.^[95]

3.5.1. Mechanism

IPMCs can be viewed as a simple double layer high surface area parallel plate capacitor with the membrane (typically negatively charged in traditional IPMCs), containing the electrolyte, squeezed between the electrodes (Figure 4A). Upon excitation with voltage (typically 1–5 V), migration of cations (and anions) to the cathode (and anode) causes swelling of

cation-reach clusters and shrinkage of other side of the membrane–electrode boundary layer.^[98] This unbalanced stress in the membrane causes the structure to bend (Figure 4E). In Nafion-based IPMCs, the initial fast response of the actuator is followed by a back-relaxation. It is believed that the back-relaxation is due to the pressure in the strained regions of the polymer matrix which squeezes water molecules out of the cation-reach clusters.^[96,98] Reversing the voltage polarity

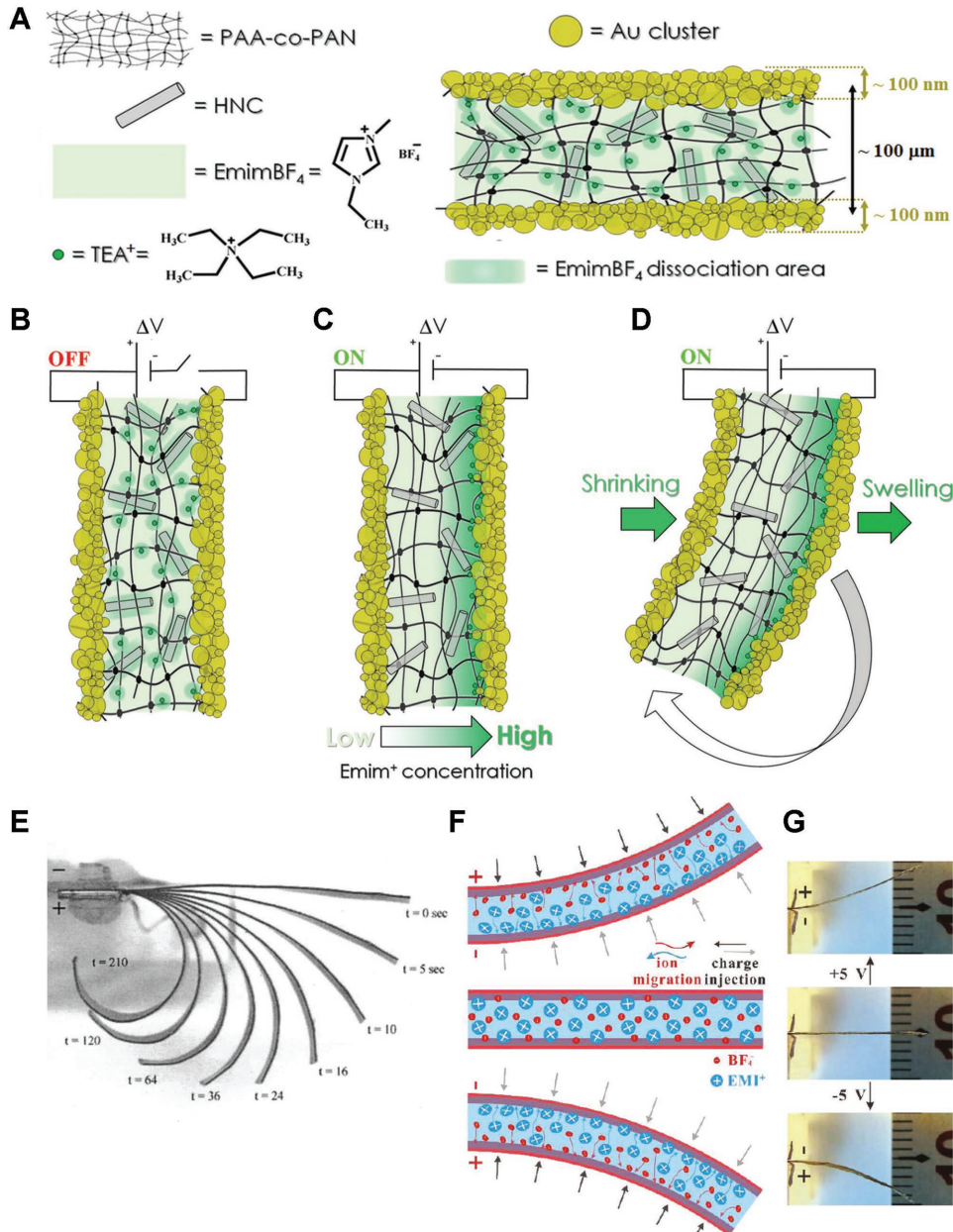


Figure 4. A) Structure of an ionic-gel/metal nanocomposite (IGMN). B–D) Actuation mechanism of the device in (A): actuator at open circuit (B); when an electrical stimulus is applied, both the tetraethylammonium (TEA)⁺ and 1-ethyl-3-methylimidazolium (EMIM)⁺ cations migrate toward the cathode (C); the differential swelling at the anodic and cathodic side of the IGMN induces the bending of the actuator toward the anode (D). E) Successive photos of a Flemion-based IPMC in TBA⁺ form, actuated by 3 V DC; the sample moves continuously toward the anode and forms nearly a circle after 3.5 min with no sign of electrolysis. F,G) Electromechanical actuation mechanism of the SWNT-based actuator: actuation illustration of the bimorph configured actuator under positive (top), negative (bottom), and no (middle) extra electrical field (F); the corresponding photographs of an actuator with a positive (top), negative (bottom), and no (middle) applied voltage of 5 V (G), well confirm the electromechanical actuation mechanism. (A–D) Reproduced with permission.^[94] Copyright 2017, Wiley-VCH. (E) Reproduced with permission.^[96] Copyright 2003, American Institute of Physics. (F,G) Reproduced with permission.^[97] Copyright 2011, American Chemical Society.

inverts the bending direction and drives the relaxation process faster. In contrast, in Flemion-based IPMCs, under the same experimental conditions, the relaxation occurs in the direction of actuation. This relaxation is believed to be due to the redistribution of cations and reorientation of electric dipoles associated with the sulfonate groups which results in reduction of repulsive interactions between them.^[98] In recent designs for IPMCs, the large difference between the ionic radius of the cations and anions in nonaqueous electrolytes such ionic liquids (e.g., 1-ethyl-3-methylimidazolium tetrafluoroborate) creates the required stress gradient across the thickness of the beam for bending (Figure 4B–D,F,G). Therefore, there is no relaxation due to back diffusion of water molecules from the cation-rich clusters. Key parameters that influence the performance of IPMCs (e.g., amplitude of the actuation, bandwidth, and generated force) are electrochemical stability, mechanical compliancy and durability, electrical conductivity of the electrodes,^[3] ionic conductivity, liquid electrolyte uptake, ion-exchange capacity, mechanical stability, and stiffness of the ionic polymers,^[3] and ionic conductivity (typically higher in aqueous electrolytes compared to ionic liquids), electrochemical stability window, and volatility in air (very low for ionic liquids and very high for aqueous electrolytes) of the electrolytes.^[95]

Aqueous-electrolyte-based IPMCs are typically fast response due to their good ionic conductivity but gradual leakage of water from the actuator as well as performance degradation in air due to the evaporation of the electrolyte have limited their applications.^[95,99] Ionic liquids, in contrast, are almost nonvolatile and possess large ion radius, which can increase the bending amplitude and blocking force. In general, ionic conductivity of ionic liquids is lower than that of the aqueous electrolytes due to the higher viscosity that they exhibit (for more information, refer to the section on conducting polymers).

Nonmetallic nanomaterials such as carbon nanotubes,^[97,100–102] graphene,^[103–105] transition metal oxide powders (e.g., RuO₂),^[106] nanoporous carbon,^[107] and carbon aerogels^[108] are among the explored suitable materials for electrodes in IPMCs. These nanopowders are cheap (<\$100 kg⁻¹ for graphene now) compared to gold or platinum, easy to coat on the IPs (through casting or self-assembly), and form very compliant electrodes with high specific surface area. However, their electrical conductivity is lower than that of the gold or platinum electrodes and typically metal backing is required to boost their electrical conductivity.^[102]

The blocking force at the tip of the IPMCs (or any other bending actuator) is proportional to the dimensions of the actuator as the following equation suggests^[100]

$$F_b \propto \frac{wt^2}{l} \quad (8)$$

where *w*, *t*, and *l* are the width, thickness, and length of the actuator.

3.5.2. Limitations

IPMCs are among the promising actuators for industrial applications and their performance has been under improvement through research and development since their invention in

1965.^[109] Similar to conducting polymers, the actuation speed in IPMCs is a function of the capacity of the electrodes as well as the electrical and ionic conductivity of the electrodes and the ionic-polymer membrane, respectively. Due to the small electrochemical stability window of aqueous electrolytes (≈ 1.23 V), electrolysis of water can lead to catastrophe due to hydrogen and oxygen evolution reactions at the electrodes. The poor stability of aqueous-electrolyte-based IPMCs in air limits their application in devices operating in dry environments, however, ionic-liquid-based IPMCs are very stable in air but they exhibit slower response time. As mentioned, due to the actuation mechanism, there can be a drift in the bending amplitude which may require correction by a feedback-loop control system. Like any other actuators, cost is an important factor in commercializing this technology.

3.5.3. Applications

IPMCs with aqueous electrolytes are more suitable for underwater applications such as fish-like robots and artificial fins. In general, IPMCs can be used in active catheters, tactile displays, braille displays, micropumps and valves, robotic grippers, sensors, and many more. Table 10 shows the results for IPMCs made of metallic and nonmetallic electrodes.

3.6. Dielectric-Elastomer Actuators (DEAs)

Dielectric elastomers are fast response actuators that can produce large strains via excitation with an electric field. Dielectric elastomers can be viewed as parallel plate capacitors with very compliant dielectric materials that exhibit relatively large Poisson's ratio (up to 0.5) (Figure 5A).^[110] Compliant materials that can generate high strains and recover with elastic modulus of less than 10 MPa are very suitable for use as a dielectric in these actuators. Elastomers based on silicones (e.g., Nusil CF19-2186, Dow Corning HS3, Dow Corning

Table 10. Ionic-polymer/metal composites (IPMCs).

Property	Metallic electrodes	Nonmetallic electrodes
Stimulus	Voltage (charge migration)	Voltage (charge migration)
Amplitude of stimulus	<7 ^[114,115]	± 4 V ^[102]
Strain [%]	>3 ^[114,115]	8.2 ^[102]
Stress [MPa]	30 ^[98,116]	4.7 ^[102]
Strain rate [% s ⁻¹]	3.3 ^[96]	9 ^[97]
Response time ^a [s]	millisecond to second (amplitude dependent)	0.019 ^[97]
Work density [J kg ⁻¹]	<4 ^[96]	2.03 ^[97]
Power density [W kg ⁻¹]	2.6 ^[96]	244 ^[97]
Bandwidth [Hz]	100 (tested) ^[96]	33 (first resonance 30 Hz) ^[97]
Efficiency [%]	<3 ^[117]	–
Cycle life	76 000 ^[94]	–

^aThe response time is very dependent on the actuator dimensions and ionic conductivity.

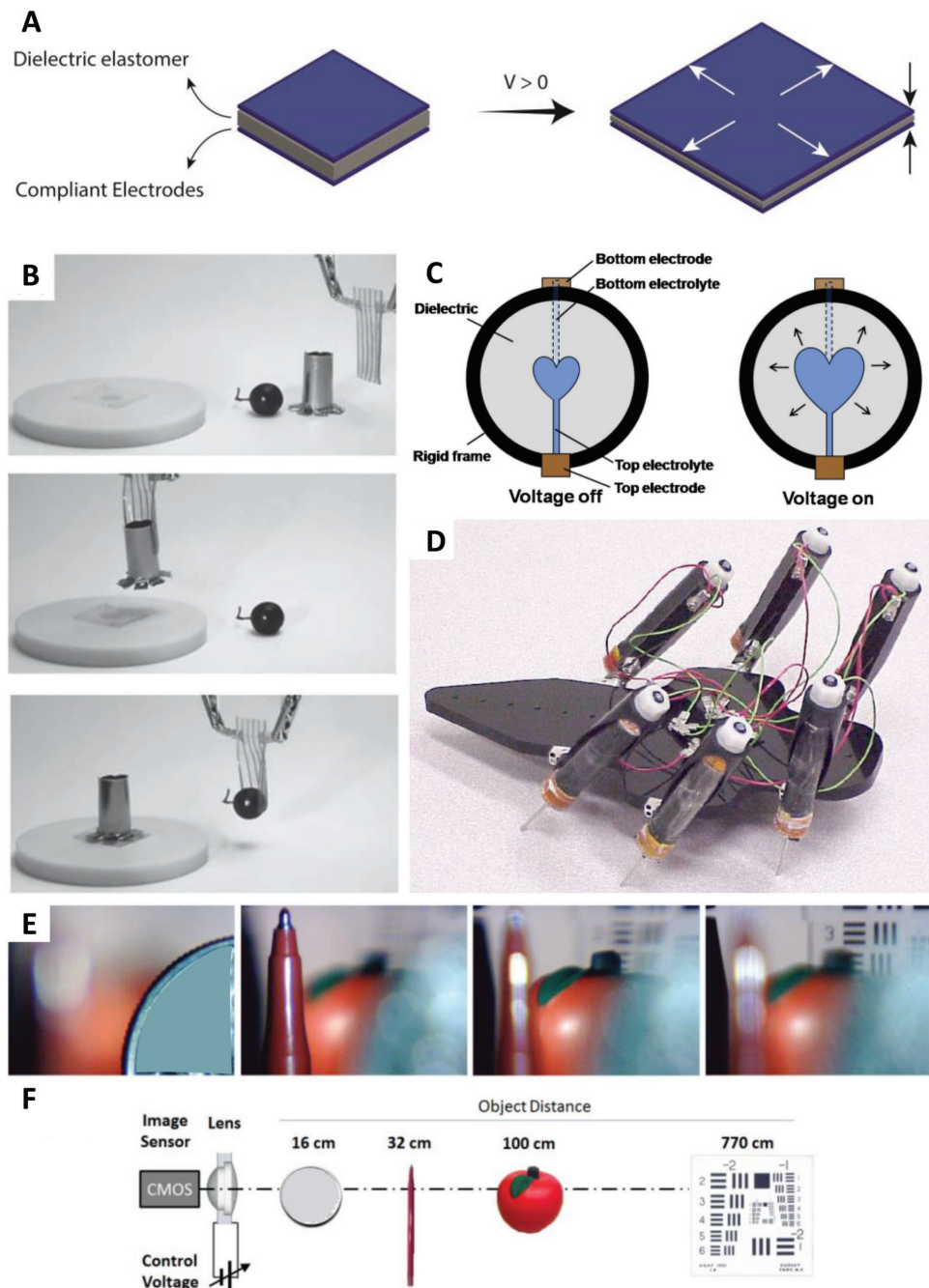


Figure 5. A) Structure of a dielectric-elastomer actuator. B) Illustration of the action of a “pick-and-place” actuator made from an elastomer beam with a few vertical fibers. The elastomer bends to conform to the shape of both the cylinder and a grape. C) A dielectric elastomer is sandwiched between two layers of an electrolytic elastomer. Both the dielectric and the electrolyte are transparent and stretchable, and the device is transparent if the electrodes are placed outside the active area of the device. Right: subject to voltage, the two layers of the electrolyte spread ions of opposite signs on the two sides of the dielectric, causing the sandwich to reduce thickness and expand area. D) Skitter robot using six rolled DE actuators. This robot has successfully demonstrated a peak speed of ≈ 70 mm s^{-1} . E) Photographic images at various focal lengths as captured by a complementary metal-oxide-semiconductor (CMOS) image sensor demonstrating the focusing capability of the lens. F) Schematic of the measurement setup used for image acquisition. (B) Reproduced with permission.^[118] Copyright 2015, Wiley-VCH. (C) Reproduced with permission.^[119] Copyright 2013, American Association for the Advancement of Science. (D) Reproduced with permission.^[120] Copyright 2002, SPIE. (E,F) Reproduced with permission.^[121] Copyright 2013, Optical Society of America.

Sylgard 186),^[111,112] acrylates (e.g., 3M VHB 4910, 3M VHB 4905),^[111,113] polyurethane (e.g., Deerfield PT6100S, Estane TPU588),^[112,122] and thermoplastic elastomer copolymers

(e.g., poly[styrene-*b*-(ethylene-*co*-butylene)-*b*-styrene] triblock copolymer)^[123] are among the typical elastomers exploited for DEAs so far. Maximum strain and electromechanical coupling

occurs when the electrodes and the dielectric are both compliant. In addition, the electrodes should be highly electrically conductive (in both the excited and relaxed states) and should be able to well retain their conductivity over millions of cycles. It is very important to minimize the added stiffness from the electrodes to the dielectric material as much as possible. Electrodes can be formed by employing carbon-based materials (e.g., carbon powder,^[124] carbon grease,^[111,124] and carbon–elastomer composites^[125]) or metallic materials (e.g., silver). Metals are better electron conductors compared to carbon-based materials but they yield small strains due to their large stiffness. Patterned metallic electrodes (such as liquid or solid metals)^[126–128] and metallic thin films on corrugated membranes^[129,130] have resolved this issue to some extent, but the strains are below 100%. Alternative materials including hydrogels with high ionic conductivity (Figure 5C),^[119] single-walled carbon nanotubes (SWNTs),^[131,132] and silver nanowires^[132] are employed as optically transparent electrodes for DEAs. For example, silver nanowire–polymer composite electrodes have shown very stable conductivity at strains as high as 140% with 65% areal actuation.^[133] Implanting metal ions such as gold, palladium, and titanium in polydimethylsiloxane (PDMS) has shown good electrical conductivity retention for strains up to 175%.^[134]

3.6.1. Mechanism

Roentgen, for the first time, observed the actuation of a sheet of natural rubber under large electric field in 1880.^[130] The applied electric field creates an attractive force (aka, Maxwell stress) between the electrodes which squeezes the compliant dielectric elastomer. Assuming the dielectric is incompressible (i.e., $(1 + \Delta l/l_0)(1 + \Delta w/w_0)(1 + \Delta t/t_0) = 1$), the change in thickness (t) leads to expansion in length (l) and/or width (w) depending on the boundary conditions. The effective pressure on the dielectric can be derived to be

$$P_{\text{eff}} = \epsilon_r \epsilon_0 \left(\frac{V}{t} \right)^2 \quad (9)$$

where ϵ_r is the relative static permittivity (aka, dielectric constant), ϵ_0 is the vacuum permittivity, V is the applied potential, and t is the thickness of the dielectric material. The effective pressure in Equation (9) is double the normalized force between plates of a parallel plate capacitor. As Equation (9) suggests, the stress scales with square of the applied electric field, however, it is limited by the break down in the dielectric which itself is a function of strain. In other words, at a constant applied voltage, as the thickness of the dielectric decreases (due to the increase in effective pressure), the electric field increases. This positive feedback loop leads to dielectric breakdown of the elastomer due to the extensive thinning of the dielectric. This phenomenon is often called electromechanical or pull-in instability. By controlling the electric charge instead of the voltage, the pull-in effect can be prevented. This technique was first used by Roentgen in his electrode-free elastomer actuators.^[136] Other methods to prevent the pull-in effect are mechanically prestraining the dielectric elastomer or utilizing interpenetrating polymer networks with a highly prestrained first component network.^[137]

In a typical DEA device, upon excitation, the elastomer elongates along the length and width due to the effective pressure exerted by the electrodes. Prestraining the elastomer in a particular direction lowers the elongation in that direction. In other words, prestraining can be used to give orientation to the strain in addition to reducing the pull-in instability. More complex actuation forms can be obtained from DEAs by patterning the electrodes or even introducing local stiffness in the elastomer (Figure 5B).^[118,138–140] Soft grippers are demonstrated by incorporating stiff fibers in the elastomer.^[118]

Different configurations for dielectric elastomers are explored which each can generate unique combination of force/strain distribution. Free-standing planar, rigid/flexible framed planar, bending, tubular and rolled, diaphragm (pressure loaded), and thickness mode are among the major categories.^[3]

3.6.2. Limitations

The relatively very high excitation voltage (typically thousands of volts) of the DEAs requires DC–DC converters, which adds to the cost and size of the device. Another limitation of DEAs is the operating voltage, which is considered to be unsafe for wearable and biomedical devices.

3.6.3. Applications

DEAs have very large bandwidth (up to kilohertz range), which makes them very attractive for application in devices such as loudspeakers,^[119] tunable optical lenses (Figure 5E,F),^[121,141–145] flapping wings,^[146] walking robots (Figure 5D),^[120,147] grippers,^[118] tactile displays,^[148,149] laser speckle reducers,^[150] microfluidics,^[151] and switches.^[152] DEAs can also be used as sensors and energy-harvesting devices when the change in capacitance, due to any change in volume of the dielectric, is harvested.^[153] Table 11 includes the results for dielectric-elastomer actuators.

Table 11. Dielectric-elastomer actuators (DEAs).

Property	Dielectric elastomers ^[154–157]
Stimulus	Voltage/electric field
Amplitude of stimulus	100–150 MV m ⁻¹ (breakdown <420 MV m ⁻¹)
Areal strain [%]	<380
Thickness strain [%]	<79
Stress [MPa]	<7.2
Work density [MJ m ⁻³]	<3.5
Tensile strength [MPa]	<7.2
Electromechanical coupling efficiency [%]	<90
Dielectric constant	2–10
Bandwidth	<1 kHz
Efficiency [%]	<90
Cycle life	>10 ⁶

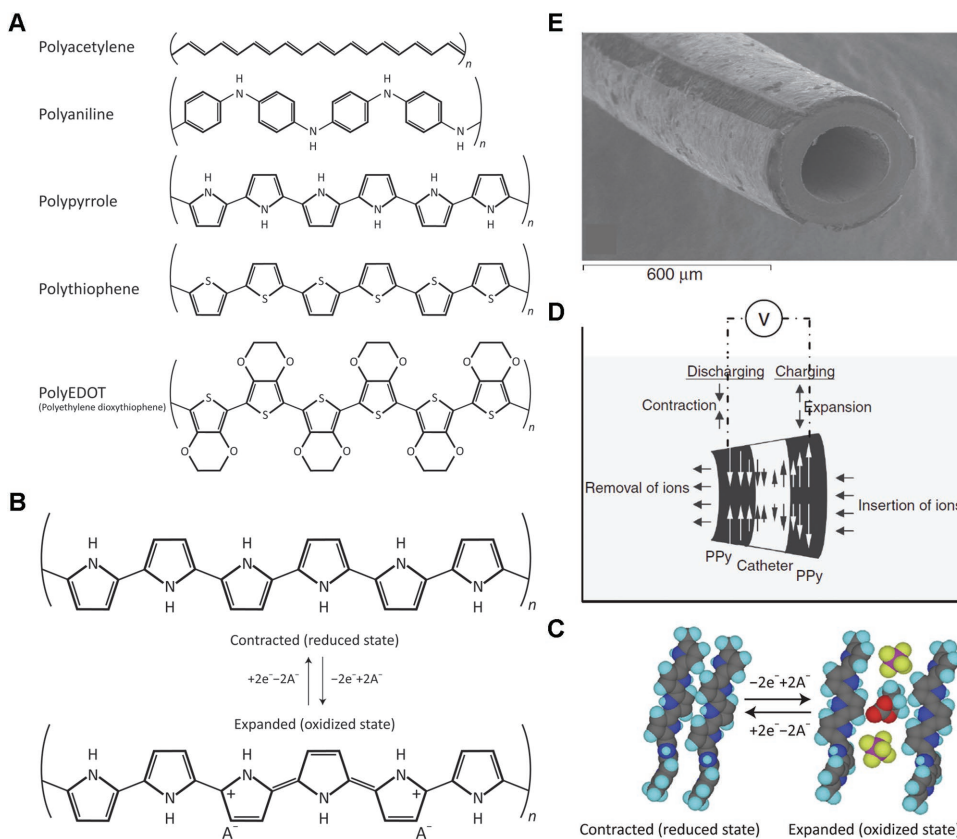


Figure 6. A) Chemical structure of some common conductive polymers. B,C) Polypyrrole oxidation/reduction reaction. Anions (A^-) diffuse into the structure to maintain the electroneutrality. D,E) Use of polypyrrole actuators on catheters to make them active: (D) Insertion of ions induces expansion in one side of the catheter while removal of ions causes contraction. The net result is bending of the catheter. A similar mechanism is responsible for the bending in trilayer conducting-polymer actuators. (E) SEM image of a catheter coated with four stripes of polypyrrole. (C) Adapted with permission.^[158] Copyright 2007, Elsevier Ltd. (D,E) Reproduced with permission.^[159] Copyright 2009, John Wiley & Sons, Ltd.

3.7. Conducting Polymers

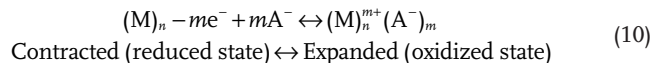
Conducting polymers are ionically and electronically conductive materials that exhibit volumetric expansion/contraction upon electrochemical oxidation/reduction in an electrolyte. Basic conducting polymers can have constituent monomers of pyrrole, thiophene, aniline, furane, indole, acetylene, azulene, carbozole, etc.,^[2,160] but only a few such as pyrrole, aniline, and thiophene and its derivatives are often used in the design of actuators (Figure 6A).^[158,161,162]

3.7.1. Mechanism

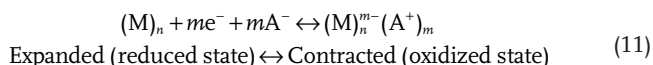
Conducting polymers mostly exhibit semiconducting behavior (bandgap > 2 eV) when undoped and conducting behavior when doped with donor or acceptor ions.^[163] The doping process can be carried out via electrochemical or chemical processes.

When subjected to potential in an electrochemical cell, conducting-polymer structures can donate or accept electrons from the metal electrode (e.g., gold, platinum, etc.) that they are deposited on. To maintain the charge neutrality in the conducting-polymer structure, flux of ions (anions or cations) from the electrolyte diffuse into the polymer structure. This

ion insertion/deinsertion generally correlates with volumetric expansion or contraction within the structure (Figure 6C). Some conducting polymers (such as polypyrrole) can be p-doped (electrons leaving the polymer chains and making them positively charged), which means that intercalation of anions from the electrolyte neutralizes the polymer structure (Figure 6B). Equation (10) shows the oxidation/reduction process for such conducting polymers



where (M) is the monomer, m is the number of electron transferred, and A^- is the anion responsible for maintaining the electroneutrality. On the opposite, some conducting polymers (such as thiophene and its derivatives) can be n-doped (electrons are injected to the structure making the chains negatively charged), which require cations for the charge neutrality inside the polymer structure. Equation (11) shows the oxidation/reduction process for such conducting polymers



The basics of actuation behavior in conducting polymers under a load can be explained by Hooke's law. Under isotonic condition, when a conducting-polymer actuator is under tensile force (F), the generated tensile strain (ε_f) is the sum of the tensile strain under no load (ε_0) and the strain due to the change in stiffness between the initial (K) and final (K') states^[164]

$$\varepsilon_f = \varepsilon_0 + F \left(\frac{1}{K'} - \frac{1}{K} \right) = \varepsilon_0 + \sigma_E \left(\frac{1}{Y_E} - \frac{1}{Y'_E} \right) \quad (12)$$

where Y_E and Y'_E are the engineering Young's modulus at the initial and final states, respectively, and σ_E is the engineering applied stress (force normalized over the cross-sectional area at the initial state).^[164] Based on experiment results, for strains of about 1%, a simple model relating the charge density (ρ) and strain (ε) is proposed (Equation (13))^[4]

$$\varepsilon = \alpha \cdot \rho + \frac{\sigma}{E} \quad (13)$$

where α is the strain to charge ratio ($\approx 10^{-10} \text{ m}^3 \text{ C}^{-1}$), σ is the applied stress, and E is the elastic modulus. However, more accurate models are proposed in which the nonlinearity and time dependency of the charging/discharging of the actuators are taken into account.^[165]

The strain that conducting-polymer actuators produce are typically on the order of few percent (Table 12).^[3,158] To amplify this strain, the following amplification mechanisms are proposed:

- (i) Bilayer bending actuators are made of an active layer (i.e., the conducting-polymer layer) and a passive layer which is attached to the active layer and causes the bending during volumetric expansion/contraction of the active layer.^[162,166–168]
- (ii) Trilayer bending actuators have one passive layer sandwiched between two active layers.^[169–172] In this configuration, both active layers are contributing to the bending motion since one layer is acting as the working electrode (expanding/shrinking in volume) and the other as the counter electrode (shrinking/expanding in volume) (similar to Figure 6D).^[169]

Table 12. Conducting-polymer actuators.

Property	Conducting polymers ^{a)}
Stimulus	Voltage (charge injection in the structure)
Amplitude of stimulus	2–10 V ^[162] (<40 V as an electrode) ^[193]
Strain [%]	2–10 ^[158] (<40) ^[194,195]
Stress [MPa]	<34 ^[158]
Strain rate [% s ⁻¹]	<12 ^[191]
Work density [M] m ⁻³	<100 ^[196]
Tensile strength [MPa]	≈100 ^[197]
Bandwidth [Hz]	<1000 ^[198]
Efficiency [%]	<18 ^[199]
Cycle life	<500 000 ^[200]
Conductivity [MS m ⁻¹]	>1 ^[201]

^{a)}All the numbers are experimental results reported in the literature.

Different designs for linear stroke conducting polymers are proposed such as interpenetrated hollow tubes,^[173,174] accordion bellows-type origami structures,^[175] nano-/microfibers,^[176–178] or even combination of bilayer and trilayer actuators.^[179]

3.7.2. Limitations

Conducting polymers can be viewed as a charge storage element in supercapacitors/batteries that expand or shrink during the charging/discharging process. Charge injection in a conducting-polymer structure is a diffusive process. Therefore, thickness of the actuator films plays an important role in actuation response time (i.e., cycling rate or bandwidth). Lowering the thickness can improve the diffusion of ions into the structure, thus increasing the cycling rate, but it can decrease the generated force. Since there is a correlation between the charge density and the strain and stress, conducting-polymer films with higher capacitance, which can be obtained by increasing the porosity, can produce larger strains and stresses.^[180] However, the degradation potential of the polymer sets a limit on the peak ion concentration in the double layer.^[181,182] Electrical conductivity of the conducting-polymer films as well as the ionic conductivity of the electrolyte can directly influence the bandwidth and the actuation performance. Higher ionic conductivity of the electrolyte and higher electrical conductivity of the conducting-polymer film enable higher currents (under potentiostatic conditions), which lead to faster charge/discharging of the films. Aqueous electrolytes are typically more ionically conductive (e.g., 73 S m⁻¹ for a 1 M sulfuric acid)^[183] compared to organic or ionic-liquid electrolytes (e.g., 1.15 S m⁻¹ for 1-ethyl-3-methylimidazolium tetrafluoroborate (EMIMBF₄)),^[184] but large ionic radius of ionic liquids can produce large peak strains and stresses.^[180] Similar to the RC time constant limit in supercapacitors,^[184] conducting-polymer actuators also have several RC time constants which each plays an important role in the actuation performance.^[185] Another limitation of conducting polymers is the delamination of the active film on the metal backing electrode (charge collector) over relatively small number of cycles.

3.7.3. Applications

Due to some of the unusual properties of conducting polymers, such as change in electrical conductivity by over seven orders of magnitude under doping/undoping,^[3] they have wide variety of applications, such as in linear/bending actuators, origami actuators, diaphragm/micropumps, light-emitting diodes, swimming robots, conducting nanowire probes, drug delivery, active catheters (Figure 6E), batteries, supercapacitors, electrochromic devices, selective membranes, braille display, microelectronics, sensors, etc.^[2,163,175,182,186–192]

3.8. Stimuli-Responsive Gels

Smart hydrogels are made of networks of cross-linked long polymer chains that swell/deswell water in response to an

external stimulus. Temperature and pH are two typical stimuli that activate hydrogels, however, some specific gels respond to other stimuli such as light intensity, electric field, specific chemicals, and biomolecules. Hydrogels generate relatively small forces, however, the relative volumetric change they can achieve is relatively large compared to what other actuators offer.

Smart hydrogels are very attractive for biomedical applications and their chemistry and mechanical properties and behavior are extensively studied. In this section, we give a brief introduction to these smart materials and discuss their applications and limitations. More information on fabrication processes and mechanical modeling of these materials can be found in the literature.^[3,202–204]

3.8.1. Mechanism

Temperature-responsive hydrogels can be divided into two major categories: lower critical solution temperature (LCST) and upper critical solution temperature (UCST). In the first group, at temperatures below LCST, the hydrogel, which has a combination of hydrophobic and hydrophilic segments in the polymer chain, swells due to domination of hydrophilic interaction with water, while at temperatures above LCST, the hydrogen bonds with water are broken and hydrophobic interactions between the polymer chains dominate, which results into the deswelling of hydrogels (Figure 7A–G). However, the case is different in UCST hydrogels, they exhibit deswelling behavior below UCST and swelling above UCST. At temperatures below UCST, strong hydrogen bonding leads to a dense complex structure, but as the temperature increases above the UCST, the hydrogen bonds break and the hydrogel starts swelling. The LCST can be increased or decreased in the hydrogels of the first group by addition of hydrophilic or hydrophobic comonomers, respectively.

In pH-responsive hydrogels, variation in pH alters the balance of hydrophobic/hydrophilic polymer chains, which leads to a large change in the properties of the gel structure. pH-responsive hydrogels can be prepared by cross-linking of polyelectrolytes (e.g., polycations and polyanions) or polymerization of pH-sensitive monomers that have ionizable functional groups. Depending on the nature of the side groups, pH sensitive hydrogels can be classified into groups of anionic and cationic hydrogels. Anionic hydrogels show maximum swelling when pK_a of ionizable groups is higher than the pH of the medium, while cationic hydrogels show maximum swelling when pK_b of the ionizable groups is lower than the pH of the medium.

Light-responsive hydrogels are typically comprised of a polymeric network with photoreactive groups. The photoreactive groups alter the properties (e.g., elasticity, swelling degree, viscosity, etc.) of the polymeric network under photoexcitation (Figure 7J). Azobenzene is one of the commonly used photoactive materials used for light-sensitive hydrogels (refer to the section of photoexcited actuators).

Electroresponsive hydrogels undergo various shape changes such as contraction, elongation, and bending in response to an electric field. Using electric field as the stimulus enables precise control of the hydrogel response. The working principle of electroresponsive hydrogels can be very similar to that of the

IPMCs. The hydrogel network has fixed charges on its network with mobile ions maintaining the electroneutrality. Upon excitation with an electric field, migration of mobile ions can generate stress gradient, thus a deformation, such as bending, in the structure.

Smart hydrogels have demonstrated energy densities up to 460 kJ m⁻³ and strains of up to 90% under 4 MPa load.^[202,205] For thin gels, time response of less than 0.5 s is achieved, which is slower than rigid actuators such as piezoactuators and shape-memory alloys, but yet it is sufficient to be used in actuators where slow response is required (e.g., drug delivery). Another remarkable property of hydrogels is their ability to be stretched up to 1200% (Figure 7H).^[206]

3.8.2. Limitations

The relatively slow response time of hydrogels as well as chemical stability and performance degradation over time are among the limitations for these smart materials.

3.8.3. Applications

Applications include artificial skins,^[207] artificial-muscle actuators,^[208] programmable structures (Figure 7I),^[209] adaptive lenses,^[119] drug delivery,^[210] and many more.^[3]

3.9. Piezoelectric Actuators

Some crystal structures with no inversion symmetry (such as perovskite and wurtzite crystal structures) have a net nonzero charge in each unit cell. This property leads to formation of electric field across the material under mechanical stress and vice versa, which is known as the piezoelectric effect. Piezoactuators have large number of commercial applications and the research field on this topic is very broad and extensively studied. Here, we briefly introduce few piezomaterials with their properties, limitations, and applications. More information can be found in review books and articles on this topic.^[210]

PZT ($\text{Pb}[\text{Zr}_{x}\text{Ti}_{1-x}]\text{O}_3$), PMN ($\text{Pb}[\text{Mg}_{1/3}\text{Nb}_{2/3}]\text{O}_3$), and PZN ($\text{Pb}[\text{Zn}_{1/3}\text{Nb}_{2/3}]\text{O}_3$) are among the materials with high electro-mechanical coupling and piezoelectric coefficient (i.e., $d_{33} = P/\sigma$ where P is the polarization and σ is the stress). PZT is a polycrystalline ceramic which is commonly used in the design of piezoelectric actuators, ultrasonic transducers, and piezoelectric resonators in general. It can generate up to 0.2% strain with electromechanical coupling of >0.5 (Table 13). In contrast, single crystal of PT (PbTiO_3)-PMN or PT-PZN exhibit better piezoelectric properties compared to those of PZT (Table 13).

The strain in the piezoceramics is relatively small and utilizing them in a bimorph structure can amplify this strain by generating bending actuation. Other forms that are developed are piezotubes (for microrobotic applications) and piezostacks (for large strain-stress actuation). Piezoactuators typically have very large bandwidth (up to 10 MHz resonance frequency), enabling application in ultrasound transducers and buzzers. Due to the reversibility of the piezoelectric effect, materials

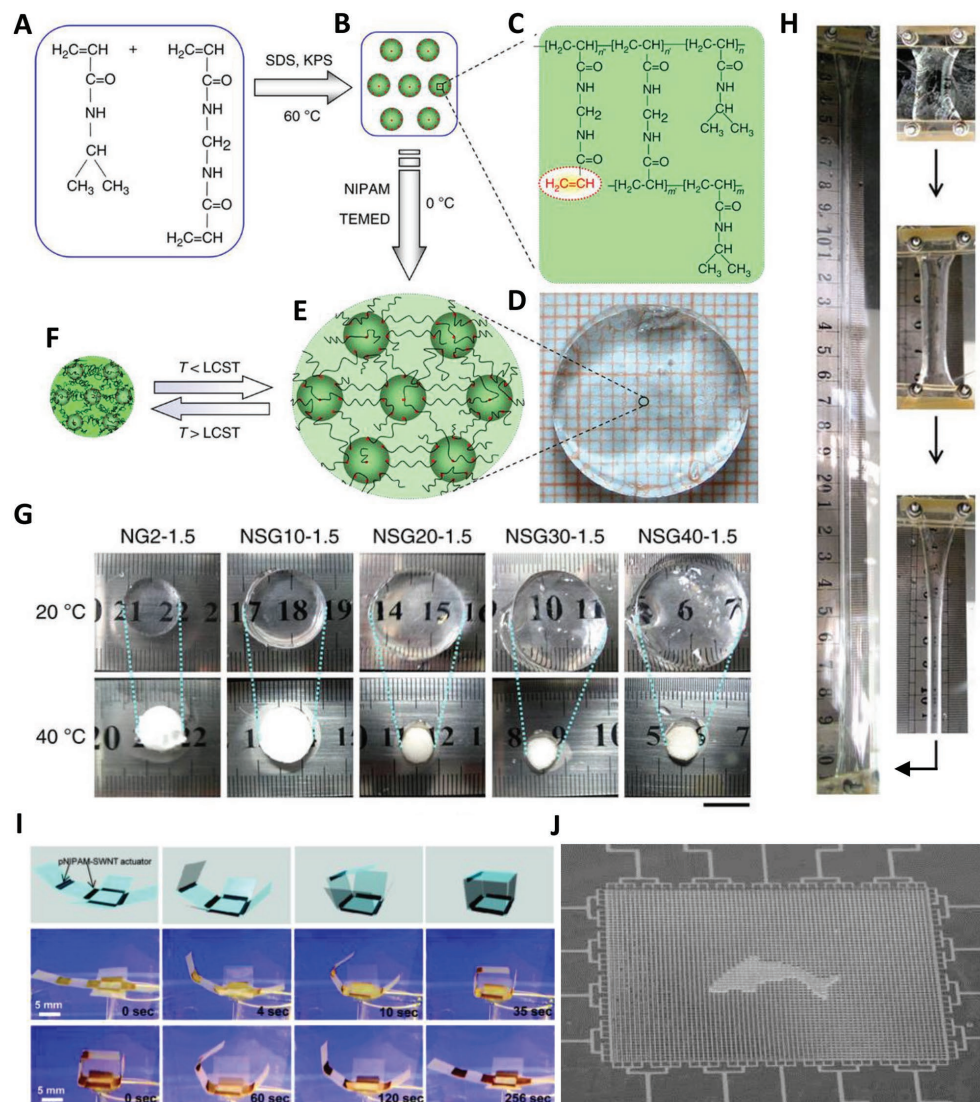


Figure 7. A–F) Hydrogel schematics with nanostructured architecture. (A) Chemical structure of *N*-isopropylacrylamide (NIPAM) and *N,N*-methylenebisacrylamide (MBA). (B) Activated nanogels (ANGs) bearing unsaturated double bonds fabricated by precipitation polymerization of NIPAM and MBA, which is initiated by potassium persulfate (KPS) in the presence of amphiphilic sodium dodecyl sulfate (SDS). (C) Chemical structure of the ANG showing the unsaturated double bonds from the unreacted parts of the MBA. (D) Optical image showing that the nanostructured hydrogels (NSG), which are fabricated from the ANGs and NIPAM with *N,N,N',N'*-tetramethylethylenediamine (TEMED) as an accelerator at 0 °C, are transparent at temperature below the LCST. Schematics of the NSG hydrogel with nanostructured architecture in the swollen state at temperature below the LCST (E), and in the shrunken state at temperature above the LCST (F). G) Optical images showing the NSG and NG hydrogel samples in swollen states at 20 °C (<LCST) and in shrunken states at 40 °C (>LCST) in pure water. Scale bar: 10 mm. H) Optical images showing the process of an NSG hydrogel being stretched to \approx 12 times its initial length in a tensile machine. I) Programmable cubes – a folding cube based on thermally responsive actuators. (Top) Fabrication scheme for folding cubes based on SWNT-poly(*N*-isopropylacrylamide) on a low-density polyethylene (pNIPAM/LDPE) bilayer actuators; (middle) cube folding by thermal actuation in 48 °C water; (bottom) the cube reversibly unfolds by cooling down the water bath in which the cube is immersed. J) A large-scale integration technology for MEMS based on the optoelectrothermic control of a temperature-sensitive hydrogel. The hydrogel itself acts as an active functional unit, i.e., as an actuator. The display comprises more than 4000 individual actuators and provides both, visual and palpable artificial impressions of a surface. (A–H) Reproduced with permission.^[206] Copyright 2013, Macmillan Publishers Limited. (I) Reproduced with permission.^[209] Copyright 2011, American Chemical Society. (J) Reproduced with permission.^[207] Copyright 2009, Wiley-VCH.

such as PZT and ZnO nanowires are demonstrated to harvest mechanical energy as well.^[212,213] By laterally coupling a vertically excited piezostack with another piezocrystal and driving the structure at its resonance frequency, voltage transformers are demonstrated from PZT piezoactuators.

3.9.1. Limitations

Small actuation strains, as well as large excitation field (MV m⁻¹ range), are two of the major undesirable characteristics of piezoceramics.

Table 13. Piezoelectric properties of some piezoelectric materials at room temperature.^[211]

Property	PZT	PMN-PT	PZN-PT
Strain [%]	0.2	0.6	1.7
Stress [MPa]	110	>100	130
Efficiency [%]	90	90	90
Electromechanical coupling (k_{33})	0.7	0.92	0.95
Piezoelectric coefficient (d_{33}) [pC N ⁻¹]	750	2500	2500

3.9.2. Applications

Micropumps, ultrasonic transducer, scanning probe microscopy, aerosol production, piezomotors, bending actuators, piezolighters, micro-/nanomanipulators, and energy-harvesting devices are some of the popular applications for piezoelectric actuators.^[211]

3.10. Electrostrictive, Magnetostrictive, and Photostrictive Actuators

Stimuli such as electric, magnetic, or electromagnetic field can actuate particular materials. Striction, the act of constricting, is the word used in combination with the stimulus to name these materials. There is a limited amount of recent research work on these materials and here, we briefly discuss their working mechanism as well as some of their properties.

3.10.1. Electrostrictive Actuators

All dielectric materials under an external electric field exhibit displacement of the atoms in the crystal lattice, which is called electrostriction. While electrostriction applies to all crystal symmetries, piezoelectric effect only applies to certain crystal structures (refer to “Piezoelectric Actuators” Section). The strain–electric field relationship in electrostrictive materials is parabolic, while in piezoelectric materials, it is linear. Lead-based ceramics such as lead magnesium niobate (PMN), lead magnesium niobate–lead titanate (PMN-PT), and lead lanthanum zirconate titanate (PLZT) are among the relaxor ferroelectrics that are highly electrostrictive. PMN actuators are very similar to piezoactuators with few important differences. PMN is a non-poled ceramic with centrosymmetric unit cells (at 0 V) and operates above the Curie temperature, which is very low compared to piezoceramics. These actuators typically exhibit hysteresis on the order of 3%, which is less than that of the piezoactuators (in a specific temperature range). Aside from ceramics, it is shown that polymers can exhibit electrostriction as well. High energy electron irradiated (HEEI) poly(vinylidene fluoride-co-trifluoroethylene) (P(VDF-TrFE)) copolymers, electrostrictive graft elastomers (G-elastomers), P(VDF-TrFE)-based terpolymers are among the well-studied electrostrictive polymers.

(HEEI) P(VDF-TrFE) copolymers are simply normal ferroelectric P(VDF-TrFE) polymers that are converted into a relaxor ferroelectric polymer (i.e., a ferroelectric material that exhibits high electrostriction) under exposure of high-energy-electron irradiations. These materials can have dielectric constants of

up to 60 (around room temperature) and exhibit strains of up to 10% (across the thickness) under 9 MV m⁻¹.^[214] It is shown that reasonably flat frequency response of up to 100 kHz is possible (with resonance peaks).^[215] The energy density generated by (HEEI) P(VDF-TrFE) copolymers can be as high as 1 MJ m⁻³, which is typically due to the relatively high elastic modulus.^[215] Electrostrictive graft elastomers can produce strains as high as 4% (across the thickness) with elastic energy density of 0.46 MJ m⁻³.^[216] With P(VDF-TrFE)-based terpolymers such as poly(vinylidene fluoride-trifluoroethylene-chlorofluoroethylene terpolymer) (P(VDF-TrFE-CFE)), terpolymer thickness strains of up to 7% is achieved.^[217] These electrostrictive polymers can generate energy density of up to 1.1 MJ m⁻³ (@4.5% strain) with longitudinal coupling factor (k_{33}) of 0.55.^[218]

It is important to note that although the strain is in a reasonable range, the actual displacement is typically less than a few hundred micrometers.

Limitations: The quadratic relationship between voltage and displacement leads to a highly nonlinear actuation behavior, which adds complexity to the controller. Some electrostrictive ceramics such as PMN exhibit capacitance up to five times higher than the piezoactuators, which increases the driving currents.

Applications: The applications are very similar to those for piezoactuators.

3.10.2. Magnetostrictive Actuators

Magnetostrictive materials can generate strain in response to excitation with magnetic field. Pure elements such as cobalt^[219] and nickel^[219] and alloys such as Terfenol-D, (Ter for terbium, Fe for iron, NOL for Naval Ordnance Laboratory, and D for dysprosium),^[220] amorphous alloy Fe₈₁Si_{3.5}B_{13.5}C₂ (under trade mark of Metglas 2605 SC),^[221] iron–aluminum alloy (from Alperm family),^[222] gallium–iron alloy (Galfenol),^[223] and 2V-Permendur (i.e., a cobalt–iron alloy containing 2% vanadium (Fe_{0.49}Co_{0.49}V_{0.02}))^[224] are among the materials that exhibit magnetostrictive behavior. Owing to its great performance, Terfenol-D (Tb_xDy_{1-x}Fe₂ with $x \approx 0.3$) is the most industrially applied magnetostrictive material and can generate strains up to 0.2–0.24% under magnetic field of 40 kA m⁻¹ and stress of 20 MPa with bandwidths up to 20 kHz.^[225] More information on the performance of other alloys of Terfenol-D and giant magnetostrictive materials can be found in the works by Liu et al.^[219] and Buschow.^[225]

A typical magnetostrictive actuator consists of a coil with magnetostrictive material as the core. Similar configuration is found in AC transformers, in which magnetostrictive phenomena is responsible for generating the 60 or 50 Hz hum.

Limitations: One of the limitations of magnetostrictive materials is the small strain that they can create (<0.5%). Aside from that, they exhibit hysteresis (magnetostriction vs strength of magnetizing field). Undesirable mechanical properties (e.g., brittleness, high stiffness) of some of these magnetostrictive materials are also limiting their applications.

Applications: Nickle and Alperm were mainly used in early sonar transducers in World War II. Later, they were replaced with Terfenol-D due to its superb performance. One of commercial products that uses Terfenol-D is the “Soundbug” by

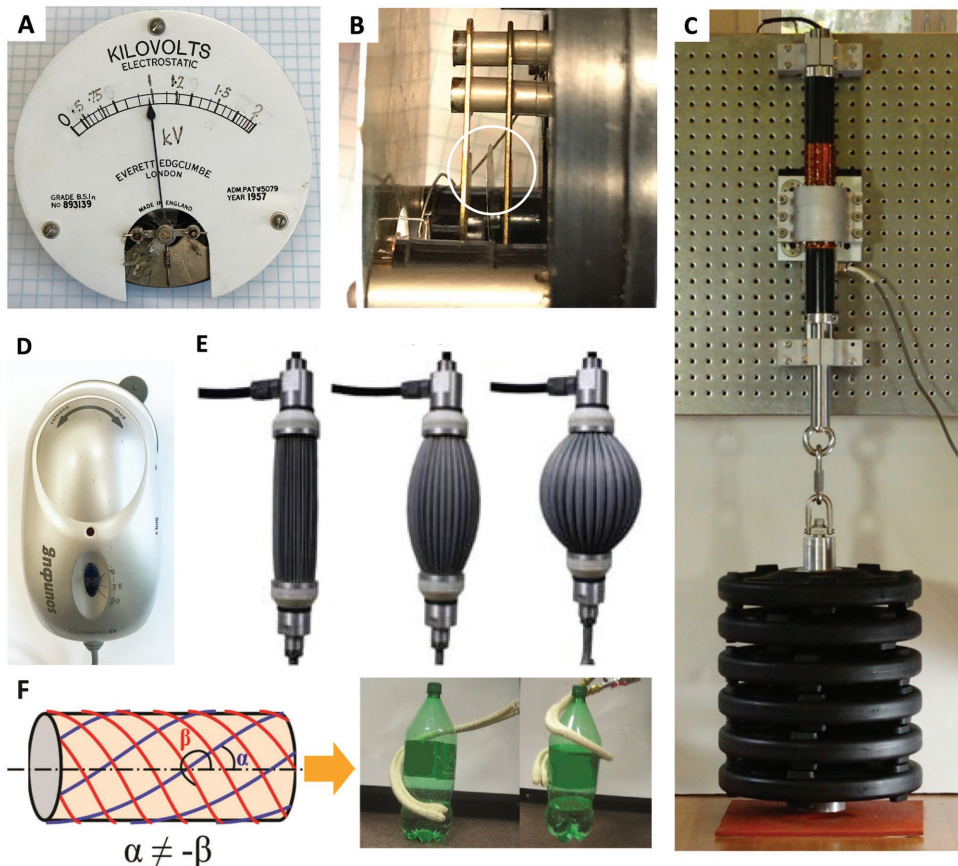


Figure 8. A) Electrostatic voltmeter. B) The electrostatic force between the middle plate and the adjacent one (shown in the white circle) controls the dial on the meter. C) X-Muscle Gen. 2 can produce 6.9 kN peak force providing 1.4 MPa active tension. It is 500 mm long and can generate a stroke of 200 mm (40%).^[226] D) Soundbug by Olympia. Terfenol-D is the actuator used in this speaker and is powerful enough to make the surface it attaches to into a speaker. E) Pleated pneumatic artificial muscle. F) A McKibben artificial muscle with asymmetric braiding angle. This asymmetry creates motions similar to what an elephant trunk can do. (C) Reproduced with permission.^[226] Copyright 2017, Nucleus Scientific. (E) Reproduced with permission.^[227] Copyright 2012, Taylor & Francis and The Robotics Society of Japan. (F) Reproduced with permission.^[228] Copyright 2015, ASME.

Olympia which converts any large thin surface to a loudspeaker by suction to the surface (Figure 8D).

3.10.3. Photostrictive Actuators

As the name suggests, light creates dimensional change in photostrictive materials. The working principle can be seen as superposition of photovoltaic effect (i.e., generation of electric field due to photoexcitation) and converse piezoelectric effect (i.e., actuation under electric field). First observation of photostriction in electrically polar materials is reported for single crystals of SbSI exhibiting up to $\approx 0.04\%$ strain (at wavelength of 700 nm) in temperatures less than 295 K.^[229] $(\text{Pb},\text{La})(\text{Zr},\text{Ti})\text{O}_3$ (aka, PLZT) ceramics, with composition formula of $\text{Pb}_{1-x}\text{La}_x(\text{Zr}_y\text{Ti}_z)_{1-x/4}\text{O}_3$, doped with WO_3 exhibit large photostriction when excited with near-UV at room temperature.^[230] It is shown that electric fields of up to 1 MV m^{-1} can be generated by a PLZT bimorph when subjected to UV radiation. PLZT can generate output strain and strain rate of up to 0.01% and $0.01\% \text{ s}^{-1}$, respectively.^[230,231] Other materials such as $\text{Sn}_2\text{P}_2\text{S}_6$ single crystals and ceramics, BiFeO_3 crystals and films, and

PbTiO_3 thin films have shown photostriction with very small strains ($<<0.01\%$). However, the response time is very fast (nanoseconds to microseconds).^[232] Polar semiconductors such as CdS single crystals, GaAs single crystals, as well as nonpolar semiconductors such as Ge and Si have shown photostriction with strains on the order of parts per million.^[232] Carbon nanotubes (both single-walled and multiwalled) and their composites have demonstrated photostriction with deformations on the order of few parts per million.^[233,234] Chalcogenide glasses have shown photostriction with strains up to 6% in As_2S_3 .^[232]

Limitations: The time response in photostrictive materials is limited by the RC time constant. Lowering the capacitance leads to smaller amplitude but faster response.

Applications: Remotely activated bimorphs, photosensors, energy-harvesting devices, and solar-powered miniature robots are some of the envisioned applications for photostrictive materials.

3.11. Photoexcited Actuators

Similar to photostrictive materials, photoexcited actuators are excited with light but with a different mechanism. The area of

photoresponsive/photoexcited materials is relatively a broad field with some overlaps with liquid crystal elastomers. In this section, we are briefly discussing the actuation mechanism and properties of these materials and more information can be found in the literature on this subject.

3.11.1. Mechanisms

Photoisomerization and photothermal actuation are two well-known mechanisms that convert light to mechanical energy. Details of these mechanisms are included in the following text:

Photoisomerization: Some organic polymers such as azobenzene, diarylethenes, spirobifluorins, and coumarins undergo *cis*–*trans* photoisomerization transitions upon radiation with high energy photons. Upon activation of *cis*–*trans* isomerization with light, the azobenzene molecular formula remains the same, however, its chemical structure changes, which causes actuation at bulk level and molecular level.^[235,236] These azobenzene molecular units can be integrated in other polymer networks, such as liquid crystalline polymers or gels,^[235,237,238] to induce photoactuation in the material. Theoretical strain of 7% is predicted for the azobenzene-based oligomer; however, up to 1% is measured in practice so far.^[239] This small strain can further be amplified with different geometries such as helix or bimorph. Up to 7 MPa is achieved for stretched azobenzene liquid crystalline polymer actuators.^[240] Energy conversion efficiency of 10% is estimated under assumption of 100% quantum efficiency for these materials.^[236]

Limitations: The generated strain is relatively small and the activation light is typically UV, in which combination of these two can limit the application in ambient-light-driven devices. Aside from these, the time response is relatively slow (on the order of seconds), which may require a long time UV exposure.

Aside from organic polymers, spin-crossover molecular crystals can also generate strain (<1.5%) but at very low temperatures (tens of Kelvin). More information on this category can be found in ref. [241].

Applications: Applications include bending actuators,^[242] switches,^[242] light-driven wheels/motors,^[239] and light/shadow-activated valves.^[239]

Photothermal Actuation: Absorption of light on the surface some materials can create stress by formation of localized heat. Similar to metallic bimorphs, if one side has a different thermal expansion, bending can occur. This idea is implemented in atomic force microscopy (AFM) to overcome some of the limitations of piezoacoustic excitation. It is demonstrated that AFM cantilevers, typically made of silicon or silicon nitride, coated with a metal can be excited with a blue laser (405 nm) to resonate the cantilever.^[243]

3.12. Electrostatic Actuators

Electrostatic actuators can be seen as dielectric-free parallel plate capacitors. The attractive force between the plates creates stress on the plates, which is half of the force experienced in dielectric elastomers (Equation (9)). This attractive force can generate strain in the plates depending on how the plates

are anchored. The normal stress on the plates scales with the square of applied electric field (Equation (9)), therefore, to be able to operate at low voltages, the gap between the plates should be very small. For such reason, their size is typically very small (micrometer range) which have made them very attractive in MEMS and nano-electromechanical systems (NEMS). Typically, the force and displacement generated by these actuators are very small (10^{-6} – 10^{-3} N or m range) but the bandwidth is on the order of tens of kilohertz.^[244] Normalized force of 35 kN m⁻² with peak strains of up to 10% and power density of 17 W kg⁻¹ is achieved for stacked, variable capacitance motor with active slider (SVCMA) actuators.^[245]

3.12.1. Limitations

Small displacement, large operating voltage for macroscopic actuators, and pull-in instability are some of the limitations of electrostatic actuators.

3.12.2. Applications

Applications include comb drivers, inkjet printer head, vacuum resonators, capacitive pressure sensors, micropumps, electrostatic loudspeakers, electrostatic voltmeters (Figure 8A,B), and radio frequency (RF) switches are among the popular applications for electrostatic actuators.^[246]

3.13. Pneumatic Actuators

Pneumatic actuators are one of the most applied actuators in the industry that work on a simple mechanism: pressurization of a fluid in an expandable chamber. The chamber can be either a piston-cylinder device or an elastically deformable one (e.g., a balloon). In this section, we briefly discuss different designs for the second category and their performance results. More detailed reviews can be found in refs. [247–249].

Similar to other actuators, pneumatic actuators can provide linear, torsional, and bending actuation. The linear actuation can be achieved in different design architectures including enclosed bladders (aka, pneumatic artificial muscles), bellows, and elastic membranes. Pneumatic artificial muscles can be divided into four major categories: braided muscle, netted muscle, pleated muscle, and embedded muscle.^[249]

Braided muscles were originally invented by Dr. O. Häfner, a physician at the Heidelberg University, in 1948. It was further developed by Dr. Joseph Laws McKibben (an atomic physicist) for use in real-life applications in 1952. The muscle is made of a very compliant tube (aka, bladder) enclosed in a braiding jacket. Upon pressurization of the bladder, due to the confinement by the braids, any volumetric expansion from the bladder translates into a linear actuation. Different braiding geometries can produce combination of linear, torsional, and bending actuation (Figure 8F).^[228]

Netted muscles are similar to braided muscles in design, however, instead of using tightly woven braiding, large hole mesh is woven around the bladder. The three major types of

netted muscles are Yarlott, RObotic Muslce ACtuator (ROMAC), and Kukolj.

Pleated muscles have bladders that are structured like a basic “origami.” Therefore, no elastic expansion of the bladder is occurring here (Figure 8E). As a result, minimum energy is spent on expanding the membrane.

Embedded muscles, unlike the first two categories, have the load carrying elements embedded in the bladder. Morin muscle, Baldwin muscle, under pressure artificial muscles (UPAM), and Paynter knitted muscle are few examples for this category.

PAMs can generate power densities of up to 10 kW kg^{-1} , which is relatively a high number compared to that of other actuators.

The other important category of pneumatic actuators is bending pneumatic actuators. Their working principle is simply on asymmetric volumetric expansion of a soft bladder. This asymmetric volumetric expansion can be achieved by pressurizing the soft bladder nonuniformly or by adding stiffness to different sections of bladder. This category is very popular and often is considered as a subcategory of soft robotics.^[250]

3.13.1. Limitations

One of the major limitations of PAMs is their limited portability due to the large space that the fluid tank (e.g., pressurized gas bottle) often takes. Different mechanisms are explored such as burning liquids/solids^[251] with high liquid/solid to gas expansion ratio but it requires constant replenishment of fuel.

3.13.2. Applications

Robotic gripper arms, soft manipulators, robotic arms/legs, soft-bodied robots are some of the applications for PAMs. Table 14 includes some results for PAMs.

3.14. Other Actuators

3.14.1. Bioinspired

Scaling of actuators to micro- or nanoscale can be challenging and sometimes impossible. In this case, nature can be a good

Table 14. Pneumatic artificial muscles.

Property	PAMs ^[247,249]
Stimulus	Fluid pressure
Amplitude of stimulus	Up to 1 MPa
Strain [%]	15
Force [N]	6 (3.4 MPa normalized to the diameter)
Peak actuation speed [mm s ⁻¹]	350
Power density [kW kg ⁻¹]	10
Work density [MJ m ⁻³]	0.5
Cycle life	30 000 tested, >100 000 expected

inspiration source. For example, bacterial flagellum is a sub-micrometer size proton gradient actuator which has not yet been mimicked efficiently. The rotary flagella are capable of propelling bacteria by a remarkable 60 cell lengths s⁻¹ which is higher than the peak 25 body lengths s⁻¹ for a cheetah. Utilizing these, tiny microactuators can be used to provide micropropellers for microrobotics. In fact, it is shown that spermatozoa can be used as the functional component of robotic microswimmers.^[252]

3.14.2. Phase-Change Effect

The Atmos torsional pendulum clocks are actuated using the temperature induced volume change of a liquid/vapor (e.g., high molecular weight alcohol) contained within a pleated metal bellows. A mechanical full wave rectifier (absolute value function) causes the spring in these clocks to be wound up for both temperature increases and decreases. Indeed, a 0.5 K change in temperature per day is sufficient to keep these clocks running.

3.14.3. Lorentz Force

Actuators exploiting the force generated when an electrical current interacts with an orthogonal magnetic field to produce a mutually orthogonal force are variously known as voice coil actuators or Lorentz force actuators. The force densities achievable by these actuators are limited by the current densities of the electrical conductor and the magnetic flux density of the source of the magnetic field (e.g., a permanent magnet). With moderate cooling, copper and silver wires can sustain current densities of between 10^7 and 10^8 A m^{-2} . Existing high energy density permanent magnets (e.g., NdFeB) have magnetic energy densities of around 300 kJ m^{-3} . By exploiting efficient magnetic circuits (e.g., Halbach arrays), solid state cooling (e.g., using graphene), linear Lorentz force actuators (e.g., the X-muscle shown in Figure 8C), generating sustained force densities of around 350 kN m^{-2} (i.e., similar to the peak stress achieved by mammalian skeletal muscle) is now possible.^[253]

4. Conclusion and Perspective

For thousands of years, the only controllable, fast, reversible actuator available on the planet was biological muscle. Advances in technology have led to the creation of numerous types of muscle-like actuators (artificial muscles) that are used in the industry to replace human muscle for some specific tasks. The artificial-muscle actuator performance metrics of force density, power density, peak strain, bandwidth, low cost, cycle life, and efficiency have individually exceeded those found in biological muscles, but as yet, no artificial muscle has matched those metrics simultaneously.

The very long cycle life of the muscle (hundreds of years) is achieved because muscle contains in every muscle cell not only the code in DNA specifying its design but also the protein fabrication machinery for its manufacture and regeneration

(the contractile proteins within most muscle fibers regenerate themselves every few months).

In addition, real muscles have the ability to modify their performance characteristics based on load and other environmental conditions. For example, the molecular structure of the heads of myosin proteins in the muscles of weight lifters, runners, and other athletes, changes as a function of training to produce muscle fibers having different contraction rates and load sustainability durations.

All of these characteristics are well beyond the anticipated capabilities of next generation artificial-muscle technologies. This remains a major but very important challenge for future.

Supporting Information

Supporting Information is available from the Wiley Online Library or from the author.

Acknowledgements

S.M.M. was supported by a Natural Sciences and Engineering Research Council of Canada (NSERC) Alexander Graham Bell Graduate Fellowship for his PhD.

Note: Figure 8 was revised after initial publication online.

Conflict of Interest

I.W.H. is the founder and has equity in a startup company (Nucleus Scientific) developing electric motors.

Keywords

actuators, artificial muscles, high-performance actuators, novel artificial muscles

Received: August 5, 2017

Revised: September 10, 2017

Published online: December 18, 2017

- [1] S. M. Mirvakili, *Niobium Nanowire Yarns and Their Application as Artificial Muscle*, University of British Columbia, Master Thesis, Vancouver, Canada **2013**.
- [2] *Electroactive Polymer (EAP) Actuators as Artificial Muscles: Reality, Potential, and Challenges*, 2nd ed. (Ed: Y. Bar-Cohen), SPIE, Bellingham, WA, USA **2004**.
- [3] *Electromechanically Active Polymers – A Concise Reference* (Ed: F. Carpi), Springer International Publishing, Switzerland **2016**.
- [4] J. D. W. Madden, N. A. Vandestee, P. A. Anquetil, P. G. A. Madden, A. Takshi, R. Z. Pytel, S. R. Lafontaine, P. A. Wieringa, I. W. Hunter, *IEEE J. Oceanic Eng.* **2004**, 29, 706.
- [5] J. Kelly, *Gunpowder: Alchemy, Bombards, and Pyrotechnics: The History of the Explosive That Changed the World*, Basic Books, New York, USA **2004**.
- [6] C. V. Anderson, *Sci. Rep.* **2016**, 6, 18625.
- [7] P. Chai, D. Millard, *J. Exp. Biol.* **1997**, 200, 2757.
- [8] R. D. Stevenson, R. K. Josephson, *J. Exp. Biol.* **1990**, 149, 61.
- [9] R. J. Full, M. S. Tu, *J. Exp. Biol.* **1990**, 148, 129.

- [10] R. J. Full, in *Comprehensive Physiology*, (Ed.: D. M. Pollock) John Wiley & Sons, Inc., **1997**, p. 853.
- [11] L. C. Rome, D. Swank, *J. Exp. Biol.* **1992**, 171, 261.
- [12] M. Burrows, *Nature* **2003**, 424, 509.
- [13] M. Burrows, *J. Neurophysiol.* **2007**, 97, 320.
- [14] M. Burrows, *J. Exp. Biol.* **2009**, 212, 2844.
- [15] O. Sotavalta, *Biol. Bull.* **1953**, 104, 439.
- [16] *The Uses of the Future in Early Modern Europe* (Eds: A. Brady, E. Butterworth), Routledge, New York **2009**.
- [17] C. S. Haines, M. D. Lima, N. Li, G. M. Spinks, J. Foroughi, J. D. W. Madden, S. H. Kim, S. Fang, M. J. de Andrade, F. Göktepe, Ö. Göktepe, S. M. Mirvakili, S. Naficy, X. Lepró, J. Oh, M. E. Kozlov, S. J. Kim, X. Xu, B. J. Swedlove, G. G. Wallace, R. H. Baughman, *Science* **2014**, 343, 868.
- [18] S. M. Mirvakili, A. R. Ravandi, I. W. Hunter, C. S. Haines, N. Li, J. Foroughi, S. Naficy, G. M. Spinks, R. H. Baughman, J. D. W. Madden, *Proc. SPIE* **2014**, 9056, 905601.
- [19] S. M. Mirvakili, I. W. Hunter, *Adv. Mater.* **2017**, 29, 1604734.
- [20] C. S. Haines, N. Li, G. M. Spinks, A. E. Aliev, J. Di, R. H. Baughman, *Proc. Natl. Acad. Sci. USA* **2016**, 113, 11709.
- [21] M. Hiraoka, K. Nakamura, H. Arase, K. Asai, Y. Kaneko, S. W. John, K. Tagashira, A. Ormote, *Sci. Rep.* **2016**, 6, 36358.
- [22] S. Hyeong Kim, M. D. Lima, M. E. Kozlov, C. S. Haines, G. M. Spinks, S. Aziz, C. Choi, H. Jun Sim, X. Wang, H. Lu, D. Qian, J. D. W. Madden, R. H. Baughman, S. Jeong Kim, *Energy Environ. Sci.* **2015**, 8, 3336.
- [23] S. Sharifi, G. Li, *Soft Matter* **2015**, 11, 3833.
- [24] S. M. Mirvakili, I. W. Hunter, *Proc. SPIE* **2016**, 9798, 97981L.
- [25] T. Arakawa, K. Takagi, K. Tahara, K. Asaka, *Proc. SPIE* **2016**, 9798, 97982W.
- [26] A. E. Aliev, J. Oh, M. E. Kozlov, A. A. Kuznetsov, S. Fang, A. F. Fonseca, R. Ovalle, M. D. Lima, M. H. Haque, Y. N. Gartstein, M. Zhang, A. A. Zakhidov, R. H. Baughman, *Science* **2009**, 323, 1575.
- [27] M. Arjadi, M. Sitti, *ACS Nano* **2016**, 10, 10202.
- [28] Q. Zhao, J. W. C. Dunlop, X. Qiu, F. Huang, Z. Zhang, J. Heyda, J. Dzubiella, M. Antonietti, J. Yuan, *Nat. Commun.* **2014**, 5, 5293.
- [29] H. Arazoe, D. Miyajima, K. Akaike, F. Araoka, E. Sato, T. Hikima, M. Kawamoto, T. Aida, *Nat. Mater.* **2016**, 15, 1084.
- [30] Y. Hu, G. Wu, T. Lan, J. Zhao, Y. Liu, W. Chen, *Adv. Mater.* **2015**, 27, 7867.
- [31] D. Kim, H. S. Lee, J. Yoon, *Sci. Rep.* **2016**, 6, 20921.
- [32] X. Zhang, Z. Yu, C. Wang, D. Zarrouk, J.-W. T. Seo, J. C. Cheng, A. D. Buchan, K. Takei, Y. Zhao, J. W. Ager, J. Zhang, M. Hettick, M. C. Hersam, A. P. Pisano, R. S. Fearing, A. Javey, *Nat. Commun.* **2014**, 5, 2983.
- [33] Y. Hu, T. Lan, G. Wu, Z. Zhu, W. Chen, *Nanoscale* **2014**, 6, 12703.
- [34] L. Chen, C. Liu, K. Liu, C. Meng, C. Hu, J. Wang, S. Fan, *ACS Nano* **2011**, 5, 1588.
- [35] R. H. Baughman, C. Cui, A. A. Zakhidov, Z. Iqbal, J. N. Barisci, G. M. Spinks, G. G. Wallace, A. Mazzoldi, D. D. Rossi, A. G. Rinzler, O. Jaschinski, S. Roth, M. Kertesz, *Science* **1999**, 284, 1340.
- [36] J. Mu, C. Hou, B. Zhu, H. Wang, Y. Li, Q. Zhang, *Sci. Rep.* **2015**, 5, 9503.
- [37] S. Park, J. An, J. W. Suk, R. S. Ruoff, *Small* **2010**, 6, 210.
- [38] M. R. Islam, X. Li, K. Smyth, M. J. Serpe, *Angew. Chem., Int. Ed.* **2013**, 52, 10330.
- [39] M. Ma, L. Guo, D. G. Anderson, R. Langer, *Science* **2013**, 339, 186.
- [40] D. Copic, A. J. Hart, *ACS Appl. Mater. Interfaces* **2015**, 7, 8218.
- [41] J. Oh, M. E. Kozlov, J. Carretero-González, E. Castillo-Martínez, R. H. Baughman, *Chem. Phys. Lett.* **2011**, 505, 31.
- [42] L. Chen, M. Weng, Z. Zhou, Y. Zhou, L. Zhang, J. Li, Z. Huang, W. Zhang, C. Liu, S. Fan, *ACS Nano* **2015**, 9, 12189.

- [43] Q. Li, C. Liu, Y.-H. Lin, L. Liu, K. Jiang, S. Fan, *ACS Nano* **2015**, *9*, 409.
- [44] S. Yao, J. Cui, Z. Cui, Y. Zhu, *Nanoscale* **2017**, *9*, 3797.
- [45] H. Bi, K. Yin, X. Xie, Y. Zhou, S. Wan, F. Banhart, L. Sun, *Nanoscale* **2013**, *5*, 9123.
- [46] M. D. Lima, N. Li, M. J. de Andrade, S. Fang, J. Oh, G. M. Spinks, M. E. Kozlov, C. S. Haines, D. Suh, J. Foroughi, S. J. Kim, Y. Chen, T. Ware, M. K. Shin, L. D. Machado, A. F. Fonseca, J. D. W. Madden, W. E. Voit, D. S. Galvão, R. H. Baughman, *Science* **2012**, *338*, 928.
- [47] S. M. Mirvakili, A. Pazukha, W. Sikkema, C. W. Sinclair, G. M. Spinks, R. H. Baughman, J. D. W. Madden, *Adv. Funct. Mater.* **2013**, *23*, 4311.
- [48] K.-Y. Chun, S. H. Kim, M. K. Shin, C. H. Kwon, J. Park, Y. T. Kim, G. M. Spinks, M. D. Lima, C. S. Haines, R. H. Baughman, S. J. Kim, *Nat. Commun.* **2014**, *5*, 3322.
- [49] M. D. Lima, M. W. Hussain, G. M. Spinks, S. Naficy, D. Hagenas, J. S. Bykova, D. Tolly, R. H. Baughman, *Small* **2015**, *11*, 3113.
- [50] J. Foroughi, G. M. Spinks, G. G. Wallace, J. Oh, M. E. Kozlov, S. Fang, T. Mirfakhrai, J. D. W. Madden, M. K. Shin, S. J. Kim, R. H. Baughman, *Science* **2011**, *334*, 494.
- [51] J. A. Lee, N. Li, C. S. Haines, K. J. Kim, X. Lepró, R. Ovalle-Robles, S. J. Kim, R. H. Baughman, *Adv. Mater.* **2017**, *29*, 1700870.
- [52] S. M. Mirvakili, I. W. Hunter, *ACS Appl. Mater. Interfaces* **2017**, *9*, 16321.
- [53] P. Chen, Y. Xu, S. He, X. Sun, S. Pan, J. Deng, D. Chen, H. Peng, *Nat. Nanotechnol.* **2015**, *10*, 1077.
- [54] A. J. Grodzinsky, *Fields, Forces, and Flows in Biological Systems*, Garland Science, New York **2011**.
- [55] J. A. Lee, Y. T. Kim, G. M. Spinks, D. Suh, X. Lepró, M. D. Lima, R. H. Baughman, S. J. Kim, *Nano Lett.* **2014**, *14*, 2664.
- [56] A. Mirabedini, S. Aziz, G. M. Spinks, J. Foroughi, *Soft Rob.* **2017**, <https://doi.org/10.1089/soro.2016.0057>.
- [57] H. Cheng, Y. Hu, F. Zhao, Z. Dong, Y. Wang, N. Chen, Z. Zhang, L. Qu, *Adv. Mater.* **2014**, *26*, 2909.
- [58] S. He, P. Chen, L. Qiu, B. Wang, X. Sun, Y. Xu, H. Peng, *Angew. Chem.* **2015**, *127*, 15093.
- [59] J. Gong, H. Lin, J. W. C. Dunlop, J. Yuan, *Adv. Mater.* **2017**, *29*, 1605103.
- [60] Y. Shang, X. He, C. Wang, L. Zhu, Q. Peng, E. Shi, S. Wu, Y. Yang, W. Xu, R. Wang, S. Du, A. Cao, Y. Li, *Adv. Eng. Mater.* **2015**, *17*, 14.
- [61] X. Huang, G. Liu, X. Wang, *Adv. Mater.* **2012**, *24*, 1482.
- [62] I. Agnarsson, A. Dhinojwala, V. Sahni, T. A. Blackledge, *J. Exp. Biol.* **2009**, *212*, 1990.
- [63] A. Ölander, *J. Am. Chem. Soc.* **1932**, *54*, 3819.
- [64] M. Kohl, *Shape Memory Microactuators*, Springer Science & Business Media, Springer-Verlag, Berlin, Heidelberg **2004**, <http://www.springer.com/us/book/9783540206354>.
- [65] J. Mohd Jani, M. Leary, A. Subic, M. A. Gibson, *Mater. Des.* **2014**, *56*, 1078.
- [66] W. Huang, *Mater. Des.* **2002**, *23*, 11.
- [67] W. J. Buehler, J. V. Gilfrich, R. C. Wiley, *J. Appl. Phys.* **1963**, *34*, 1475.
- [68] F. E. Wang, W. J. Buehler, S. J. Pickart, *J. Appl. Phys.* **1965**, *36*, 3232.
- [69] T. R. Meling, J. Odegaard, *Angle Orthod.* **1998**, *68*, 357.
- [70] G. Welsch, R. Boyer, E. W. Collings, *Materials Properties Handbook: Titanium Alloys*, ASM International, Materials Park, OH, USA **1993**.
- [71] K. Otsuka, C. M. Wayman, *Shape Memory Materials*, Cambridge University Press, Cambridge, UK **1999**.
- [72] I. W. Hunter, S. Lafontaine, J. M. Hollerbach, P. J. Hunter, in *1991 Proc. IEEE Micro Electro Mechanical Systems*, IEEE, Nara, Japan **1991**, pp. 166–170.
- [73] I. Hunter, S. R. Lafontaine, *US5092901 A*, **1992**.
- [74] I. W. Hunter, S. Lafontaine, in *IEEE Technical Digest on Solid-State Sensor and Actuator Workshop*, IEEE, Hilton Head Island, SC, USA **1992**, pp. 178–185.
- [75] G. Lim, K. Park, M. Sugihara, K. Minami, M. Esashi, *Sens. Actuators, A* **1996**, *56*, 113.
- [76] A. T. Tung, B.-H. Park, D. H. Liang, G. Niemeyer, *Sens. Actuators, A* **2008**, *147*, 83.
- [77] A. T. Tung, B. H. Park, G. Niemeyer, D. H. Liang, *IEEE/ASME Trans. on Mechatronics* **2007**, *12*, 439.
- [78] Y. Haga, Y. Tanahashi, M. Esashi, in *Proc. MEMS 98 IEEE*, IEEE, Heidelberg, Germany **1998**, pp. 419–424.
- [79] Y. Haga, M. Esashi, S. Maeda, in *Proc. IEEE 13th Annual Int. Conf. on Micro Electro Mechanical Systems*, IEEE, Miyazaki, Japan **2000**, pp. 181–186.
- [80] S.-H. Song, J.-Y. Lee, H. Rodrigue, I.-S. Choi, Y. J. Kang, S.-H. Ahn, *Sci. Rep.* **2016**, *6*, 21118.
- [81] K. J. Gabriel, W. S. N. Trimmer, J. A. Walker, *Sens. Actuators* **1988**, *15*, 95.
- [82] S. M. Mirvakili, I. W. Hunter, *Proc. SPIE* **2017**, *10163*, 101630S.
- [83] J. K. Paik, E. Hawkes, R. J. Wood, *Smart Mater. Struct.* **2010**, *19*, 125014.
- [84] D. J. Hartl, D. C. Lagoudas, *Proc. Inst. Mech. Eng., Part G* **2007**, *221*, 535.
- [85] D. Hwang, T. Higuchi, *IEEE/ASME Trans. on Mechatronics* **2014**, *19*, 1625.
- [86] A. D. Johnson, *US4965545 A*, **1990**.
- [87] D. E. Hodgson, W. H. Ming, R. J. Biermann, in *ASM Handbook*, ASM International, Materials Park, OH, USA **1990**, p. 897.
- [88] C. M. Jackson, H. J. Wagner, R. J. Wasilewski, *The Alloy with a Memory, 55-Nitinol: Its Physical Metallurgy, Properties, and Applications*, NASA, Washington, United States **1972**.
- [89] Y. Song, X. Chen, V. Dabade, T. W. Shield, R. D. James, *Nature* **2013**, *502*, 85.
- [90] B. Holschuh, E. Obopta, D. Newman, *IEEE/ASME Trans. on Mechatronics* **2015**, *20*, 1264.
- [91] C. Liu, H. Qin, P. T. Mather, *J. Mater. Chem.* **2007**, *17*, 1543.
- [92] F. Carpi, E. Smela, *Biomedical Applications of Electroactive Polymer Actuators*, John Wiley & Sons, Ltd., Chichester, UK **2009**.
- [93] C. Jo, D. Pugal, I.-K. Oh, K. J. Kim, K. Asaka, *Prog. Polym. Sci.* **2013**, *38*, 1037.
- [94] Y. Yan, T. Santaniello, L. G. Bettini, C. Minnai, A. Bellacicca, R. Porotti, I. Denti, G. Faraone, M. Merlini, C. Lenardi, P. Milani, *Adv. Mater.* **2017**, *29*, 1606109.
- [95] L. Kong, W. Chen, *Adv. Mater.* **2014**, *26*, 1025.
- [96] S. Nemat-Nasser, Y. Wu, *J. Appl. Phys.* **2003**, *93*, 5255.
- [97] J. Li, W. Ma, L. Song, Z. Niu, L. Cai, Q. Zeng, X. Zhang, H. Dong, D. Zhao, W. Zhou, S. Xie, *Nano Lett.* **2011**, *11*, 4636.
- [98] S. Nemat-Nasser, *J. Appl. Phys.* **2002**, *92*, 2899.
- [99] M. Shahinpoor, K. J. Kim, *J. Intell. Mater. Syst. Struct.* **2002**, *13*, 369.
- [100] K. Mukai, K. Asaka, K. Kiyohara, T. Sugino, I. Takeuchi, T. Fukushima, T. Aida, *Electrochim. Acta* **2008**, *53*, 5555.
- [101] V. Palmre, J. Torop, M. Arulepp, T. Sugino, K. Asaka, A. Jänes, E. Lust, A. Aabloo, *Carbon* **2012**, *50*, 4351.
- [102] S. Liu, Y. Liu, H. Cebeci, R. G. de Villoria, J.-H. Lin, B. L. Wardle, Q. M. Zhang, *Adv. Funct. Mater.* **2010**, *20*, 3266.
- [103] J. Kim, J.-H. Jeon, H.-J. Kim, H. Lim, I.-K. Oh, *ACS Nano* **2014**, *8*, 2986.
- [104] X. Xie, L. Qu, C. Zhou, Y. Li, J. Zhu, H. Bai, G. Shi, L. Dai, *ACS Nano* **2010**, *4*, 6050.
- [105] J. Kim, S.-H. Bae, M. Kotal, T. Stalbaum, K. J. Kim, I.-K. Oh, *Small* **2017**, *13*, 1701314.
- [106] B. Akle, S. Nawshin, D. Leo, *Smart Mater. Struct.* **2007**, *16*, S256.
- [107] V. Palmre, D. Brandell, U. Mäeorg, J. Torop, O. Volobujeva, A. Punning, U. Johanson, M. Kruusmaa, A. Aabloo, *Smart Mater. Struct.* **2009**, *18*, 095028.
- [108] V. Palmre, E. Lust, A. Jänes, M. Koel, A.-L. Peikolainen, J. Torop, U. Johanson, A. Aabloo, *J. Mater. Chem.* **2011**, *21*, 2577.
- [109] R. P. Hamlen, C. E. Kent, S. N. Shafer, *Nature* **1965**, *206*, 1149.

- [110] F. Carpi, D. De Rossi, *Mater. Sci. Eng., C* **2004**, *24*, 555.
- [111] R. Pehrine, R. Kornbluh, Q. Pei, J. Joseph, *Science* **2000**, *287*, 836.
- [112] R. Pehrine, R. Kornbluh, J. Joseph, R. Heydt, Q. Pei, S. Chiba, *Mater. Sci. Eng., C* **2000**, *11*, 89.
- [113] R. Shankar, T. K. Ghosh, R. J. Spontak, *Macromol. Rapid Commun.* **2007**, *28*, 1142.
- [114] K. J. Kim, M. Shahinpoor, *Polymer* **2002**, *43*, 797.
- [115] M. Shahinpoor, K. J. Kim, *Smart Mater. Struct.* **2005**, *14*, 197.
- [116] M. Shahinpoor, K. J. Kim, *Smart Mater. Struct.* **2001**, *10*, 819.
- [117] K. J. Kim, M. Shahinpoor, *Smart Mater. Struct.* **2003**, *12*, 65.
- [118] S. Shian, K. Bertoldi, D. R. Clarke, *Adv. Mater.* **2015**, *27*, 6814.
- [119] C. Keplinger, J.-Y. Sun, C. C. Foo, P. Rothmund, G. M. Whitesides, Z. Suo, *Science* **2013**, *341*, 984.
- [120] R. Pehrine, R. D. Kornbluh, Q. Pei, S. Stanford, S. Oh, J. Eckerle, R. J. Full, M. A. Rosenthal, K. Meijer, *Proc. SPIE* **2002**, *4695*, 126.
- [121] S. Shian, R. M. Diebold, D. R. Clarke, *Opt. Express* **2013**, *21*, 8669.
- [122] L. Petit, B. Guiffard, L. Seveyrat, D. Guyomar, *Sens. Actuators, A* **2008**, *148*, 105.
- [123] R. Shankar, T. K. Ghosh, R. J. Spontak, *Adv. Mater.* **2007**, *19*, 2218.
- [124] F. Carpi, P. Chiarelli, A. Mazzoldi, D. De Rossi, *Sens. Actuators, A* **2003**, *107*, 85.
- [125] O. A. Araromi, I. Gavrilovich, J. Shintake, S. Rosset, M. Richard, V. Gass, H. R. Shea, *IEEE/ASME Trans. on Mechatronics* **2015**, *20*, 438.
- [126] Y. Liu, M. Gao, S. Mei, Y. Han, J. Liu, *Appl. Phys. Lett.* **2013**, *103*, 064101.
- [127] L. Guo, S. P. DeWeerth, *Small* **2010**, *6*, 2847.
- [128] A. Pimpin, Y. Suzuki, N. Kasagi, *J. Microelectromech. Syst.* **2007**, *16*, 753.
- [129] M. Benslimane, P. Gravesen, P. Sommer-Larsen, *Proc. SPIE* **2002**, *4695*, 150.
- [130] M. Benslimane, H.-E. Kiil, M. J. Tryson, *Proc. SPIE* **2010**, *7642*, 764231.
- [131] W. Yuan, L. B. Hu, Z. B. Yu, T. Lam, J. Biggs, S. M. Ha, D. J. Xi, B. Chen, M. K. Senesky, G. Grüner, Q. Pei, *Adv. Mater.* **2008**, *20*, 621.
- [132] S. Shian, R. M. Diebold, A. McNamara, D. R. Clarke, *Appl. Phys. Lett.* **2012**, *101*, 061101.
- [133] S. Yun, X. Niu, Z. Yu, W. Hu, P. Brochu, Q. Pei, *Adv. Mater.* **2012**, *24*, 1321.
- [134] S. Rosset, M. Niklaus, P. Dubois, H. R. Shea, *Adv. Funct. Mater.* **2009**, *19*, 470.
- [135] W. C. Roentgen, in *Annual Physics and Chemistry Series*, Vol. 11, Sect. III (Ed: G. Wiedemann), **1880**, p. 771.
- [136] C. Keplinger, M. Kaltenbrunner, N. Arnold, S. Bauer, *Proc. Natl. Acad. Sci. USA* **2010**, *107*, 4505.
- [137] X. Niu, X. Yang, P. Brochu, H. Stoyanov, S. Yun, Z. Yu, Q. Pei, *Adv. Mater.* **2012**, *24*, 6513.
- [138] G. Kofod, W. Wirges, M. Paajanen, S. Bauer, *Appl. Phys. Lett.* **2007**, *90*, 081916.
- [139] G. Kofod, M. Paajanen, S. Bauer, *Appl. Phys. A: Mater. Sci. Process.* **2006**, *85*, 141.
- [140] J. Shintake, S. Rosset, B. Schubert, D. Floreano, H. Shea, *Adv. Mater.* **2016**, *28*, 231.
- [141] B. Jin, J.-H. Lee, Z. Zhou, G. Zhang, G.-B. Lee, H. Ren, C. Nah, *Opt. Eng.* **2016**, *55*, 017107.
- [142] F. Carpi, G. Frediani, S. Turco, D. De Rossi, *Adv. Funct. Mater.* **2011**, *21*, 4152.
- [143] L. Maffli, S. Rosset, M. Ghilardi, F. Carpi, H. Shea, *Adv. Funct. Mater.* **2015**, *25*, 1656.
- [144] S. Yun, S. Park, S. Nam, B. Park, S. K. Park, S. Mun, J. M. Lim, K.-U. Kyung, *Appl. Phys. Lett.* **2016**, *109*, 141908.
- [145] S. Yun, S. Park, B. Park, S. Nam, S. K. Park, K.-U. Kyung, *Appl. Phys. Lett.* **2015**, *107*, 081907.
- [146] T. Li, G. Li, Y. Liang, T. Cheng, J. Dai, X. Yang, B. Liu, Z. Zeng, Z. Huang, Y. Luo, T. Xie, W. Yang, *Sci. Adv.* **2017**, *3*, e1602045.
- [147] C. T. Nguyen, H. Phung, T. D. Nguyen, C. Lee, U. Kim, D. Lee, H. Moon, J. Koo, J. Nam, H. R. Choi, *Smart Mater. Struct.* **2014**, *23*, 065005.
- [148] S. Yun, S. Park, B. Park, S. K. Park, H. Prahlad, P. V. Guggenberg, K. U. Kyung, *IEEE/ASME Trans. on Mechatronics* **2014**, *19*, 1463.
- [149] X. Niu, P. Brochu, B. Salazar, Q. Pei, *Proc. SPIE* **2011**, *7976*, 797610.
- [150] "Optotune," <http://www.optotune.com/> (accessed: July 2017).
- [151] D. McCoul, C. Murray, D. Di Carlo, Q. Pei, *Proc. SPIE* **2013**, *8687*, 86872G.
- [152] B. M. O'Brien, E. P. Calius, T. Inamura, S. Q. Xie, I. A. Anderson, *Appl. Phys. A: Mater. Sci. Process.* **2010**, *100*, 385.
- [153] M. Rosenthal, N. Bonwit, C. Duncheon, J. Heim, *Proc. SPIE* **2007**, *6524*, 65241F.
- [154] M. Duduta, R. J. Wood, D. R. Clarke, *Adv. Mater.* **2016**, *28*, 8058.
- [155] P. Brochu, Q. Pei, *Macromol. Rapid Commun.* **2010**, *31*, 10.
- [156] R. D. Kornbluh, R. Pehrine, Q. Pei, R. Heydt, S. Stanford, S. Oh, J. Eckerle, *Proc. SPIE* **2002**, *4698*, 254.
- [157] J.-D. Nam, H. R. Choi, J. C. Koo, Y. K. Lee, K. J. Kim, in *Electroactive Polymers for Robotic Applications*, (Eds.: K. J. Kim, S. Tadokoro) Springer, London **2007**, pp. 37–48.
- [158] T. Mirfakhrai, J. D. W. Madden, R. H. Baughman, *Mater. Today* **2007**, *10*, 30.
- [159] T. Shoa, J. D. Madden, N. R. Munce, V. X. D. Yang, in *Biomedical Applications of Electroactive Polymer Actuators* (Eds: F. Carpi, E. Smela), John Wiley & Sons, Ltd., Chichester, United Kingdom **2009**, pp. 229–248.
- [160] T. F. Otero, *Polym. Rev.* **2013**, *53*, 311.
- [161] R. H. Baughman, *Synth. Met.* **1996**, *78*, 339.
- [162] J. D. Madden, R. A. Cush, T. S. Kanigan, I. W. Hunter, *Synth. Met.* **2000**, *113*, 185.
- [163] T. A. Skotheim, *Handbook of Conducting Polymers, Second Edition*, CRC Press, New York, USA **1997**.
- [164] G. M. Spinks, L. Liu, G. G. Wallace, D. Zhou, *Adv. Funct. Mater.* **2002**, *12*, 437.
- [165] M. Farajollahi, F. Sassani, N. Naserifar, A. Fannir, C. Plesse, G. T. M. Nguyen, F. Vidal, J. D. W. Madden, *Smart Mater. Struct.* **2016**, *25*, 115044.
- [166] G. Han, G. Shi, *Sens. Actuators, B* **2006**, *113*, 259.
- [167] T. F. Otero, J. G. Martinez, M. Fuchiwaki, L. Valero, *Adv. Funct. Mater.* **2014**, *24*, 1265.
- [168] M. Fuchiwaki, J. G. Martinez, T. F. Otero, *Adv. Funct. Mater.* **2015**, *25*, 1535.
- [169] F. García-Córdova, L. Valero, Y. Ahmed Ismail, T. Fernandez Otero, *J. Mater. Chem.* **2011**, *21*, 17265.
- [170] G. Aliche, V. Devaud, P. Renaud, G. Spinks, *J. Micromech. Microeng.* **2009**, *19*, 025017.
- [171] Q. Yao, G. Aliche, G. M. Spinks, *Sens. Actuators, A* **2008**, *144*, 176.
- [172] G. Han, G. Shi, *J. Electroanal. Chem.* **2004**, *569*, 169.
- [173] F. Vidal, C. Plesse, P.-H. Aubert, L. Beouch, F. Tran-Van, G. Palaprat, P. Verge, P. Yammine, J. Citerin, A. Kheddar, L. Sauques, C. Chevrot, D. Teyssié, *Polym. Int.* **2010**, *59*, 313.
- [174] C. Plesse, F. Vidal, D. Teyssié, C. Chevrot, *Adv. Sci. Technol.* **2008**, *61*, 53.
- [175] H. Okuzaki, T. Saido, H. Suzuki, Y. Hara, H. Yan, *J. Phys.: Conf. Ser.* **2008**, *127*, 012001.
- [176] H. Okuzaki, Y. Harashina, H. Yan, *Eur. Polym. J.* **2009**, *45*, 256.
- [177] V. Mottaghitalab, G. M. Spinks, G. G. Wallace, *Polymer* **2006**, *47*, 4996.

- [178] J. Foroughi, G. M. Spinks, G. G. Wallace, *Synth. Met.* **2009**, *159*, 1837.
- [179] M. Fuchiwaki, K. Tanaka, K. Kaneto, *Sens. Actuators, A* **2009**, *150*, 272.
- [180] P. G. A. Madden, J. D. W. Madden, P. A. Anquetil, N. A. Vandesteeg, I. W. Hunter, *IEEE J. Oceanic Eng.* **2004**, *29*, 696.
- [181] T. W. Lewis, G. M. Spinks, G. G. Wallace, A. Mazzoldi, D. De Rossi, *Synth. Met.* **2001**, *122*, 379.
- [182] W. Lu, A. G. Fadeev, B. Qi, E. Smela, B. R. Mattes, J. Ding, G. M. Spinks, J. Mazurkiewicz, D. Zhou, G. G. Wallace, D. R. MacFarlane, S. A. Forsyth, M. Forsyth, *Science* **2002**, *297*, 983.
- [183] M. Galirski, A. Lewandowski, I. Stępiak, *Electrochim. Acta* **2006**, *51*, 5567.
- [184] S. M. Mirvakili, I. W. Hunter, *Adv. Mater.* **2017**, *29*, 1700671.
- [185] S. Ebrahimi Takalloo, H. Seifi, J. D. W. Madden, *Proc. SPIE* **2017**, *10163*, 1016312.
- [186] R. R. Llinás, K. D. Walton, M. Nakao, I. Hunter, P. A. Anquetil, *J. Nanopart. Res.* **2005**, *7*, 111.
- [187] Y. Fang, X. Tan, *Sens. Actuators, A* **2010**, *158*, 121.
- [188] G. Alici, G. Spinks, N. N. Huynh, L. Sarmadi, R. Minato, *Bioinspiration Biomimetics* **2007**, *2*, S18.
- [189] T. Götsche, S. Haeberle, in *Biomedical Applications of Electroactive Polymer Actuators* (Eds: F. Carpi, E. Smela), John Wiley & Sons, Ltd., Chichester, United Kingdom **2009**, pp. 301–316.
- [190] K. K. C. Lee, N. R. Munce, T. Shoa, L. G. Charron, G. A. Wright, J. D. Madden, V. X. D. Yang, *Sens. Actuators, A* **2009**, *153*, 230.
- [191] J. Ding, L. Liu, G. M. Spinks, D. Zhou, G. G. Wallace, J. Gillespie, *Synth. Met.* **2003**, *138*, 391.
- [192] Y. Naka, M. Fuchiwaki, K. Tanaka, *Polym. Int.* **2010**, *59*, 352.
- [193] C. S. Lee, J. Joo, S. Han, S. K. Koh, *Sens. Actuators, A* **2005**, *121*, 373.
- [194] S. Hara, T. Zama, W. Takashima, K. Kaneto, *Polym. J.* **2004**, *36*, 933.
- [195] S. Hara, T. Zama, W. Takashima, K. Kaneto, *Smart Mater. Struct.* **2005**, *14*, 1501.
- [196] G. M. Spinks, V.-T. Truong, *Sens. Actuators, A* **2005**, *119*, 455.
- [197] G. M. Spinks, V. Mottaghitalab, M. Bahrami-Samani, P. G. Whitten, G. G. Wallace, *Adv. Mater.* **2006**, *18*, 637.
- [198] A. Maziz, C. Plesse, C. Soyer, C. Chevrot, D. Teyssié, E. Cattan, F. Vidal, *Adv. Funct. Mater.* **2014**, *24*, 4851.
- [199] J. D. W. Madden, *Ph.D. Thesis*, Massachusetts Institute of Technology, **2000**.
- [200] G. M. Spinks, G. G. Wallace, J. Ding, D. Zhou, B. Xi, J. Gillespie, *Proc. SPIE* **2003**, *5051*, 372.
- [201] J. Tsukamoto, *Adv. Phys.* **1992**, *41*, 509.
- [202] A. Richter, in *Hydrogel Sensors and Actuators*, (Eds.: G. Gerlach, K.-F. Arndt) Springer, Berlin **2009**, pp. 221–248.
- [203] K.-F. Arndt, F. Krahl, S. Richter, G. Steiner, in *Hydrogel Sensors and Actuators*, (Eds.: G. Gerlach, K.-F. Arndt) Springer, Berlin **2009**, pp. 69–136.
- [204] O. Okay, in *Hydrogel Sensors and Actuators*, (Eds.: G. Gerlach, K.-F. Arndt) Springer, Berlin **2009**, pp. 1–14.
- [205] R. Greiner, M. Allerdissen, A. Voigt, A. Richter, *Lab Chip* **2012**, *12*, 5034.
- [206] L.-W. Xia, R. Xie, X.-J. Ju, W. Wang, Q. Chen, L.-Y. Chu, *Nat. Commun.* **2013**, *4*, 3226.
- [207] A. Richter, G. Paschew, *Adv. Mater.* **2009**, *21*, 979.
- [208] Z. Liu, P. Calvert, *Adv. Mater.* **2000**, *12*, 288.
- [209] X. Zhang, C. L. Pint, M. H. Lee, B. E. Schubert, A. Jamshidi, K. Takei, H. Ko, A. Gillies, R. Bardhan, J. J. Urban, M. Wu, R. Fearing, A. Javey, *Nano Lett.* **2011**, *11*, 3239.
- [210] S. C. Lee, I. K. Kwon, K. Park, *Adv. Drug Delivery Rev.* **2013**, *65*, 17.
- [211] K. Uchino, *Advanced Piezoelectric Materials: Science and Technology*, Elsevier, Published by Woodhead Publishing Limited, Cambridge, UK **2010**.
- [212] S. Xu, B. J. Hansen, Z. L. Wang, *Nat. Commun.* **2010**, *1*, 1098.
- [213] Z. L. Wang, J. Song, *Science* **2006**, *312*, 242.
- [214] R. Casalini, C. M. Roland, *Appl. Phys. Lett.* **2001**, *79*, 2627.
- [215] T.-B. Xu, Z.-Y. Cheng, Q. M. Zhang, *Appl. Phys. Lett.* **2002**, *80*, 1082.
- [216] J. Su, J. S. Harrison, T. L. S. Clair, *US6515077 B1*, **2003**.
- [217] C. Huang, R. Klein, F. Xia, H. Li, Q. M. Zhang, F. Bauer, Z. Y. Cheng, *IEEE Trans. Dielectr. Electr. Insul.* **2004**, *11*, 299.
- [218] F. Xia, Z.-Y. Cheng, H. S. Xu, H. F. Li, Q. M. Zhang, G. J. Kavarnos, R. Y. Ting, G. Abdul-Sadek, K. D. Belfield, *Adv. Mater.* **2002**, *14*, 1574.
- [219] J. Liu, C. Jiang, H. Xu, *Sci. China: Technol. Sci.* **2012**, *55*, 1319.
- [220] A. E. Clark, M. Wun-Fogle, *Proc. SPIE* **2002**, *4699*, 421.
- [221] A. Hossain, M. H. Rashid, *IEEE Trans. Ind. Appl.* **1990**, *26*, 1158.
- [222] M. Wuttig, L. Dai, J. Cullen, *Appl. Phys. Lett.* **2002**, *80*, 1135.
- [223] Q. Xing, Y. Du, R. J. McQueeny, T. A. Lograsso, *Acta Mater.* **2008**, *56*, 4536.
- [224] M. R. Karafi, Y. Hojjat, F. Sassani, M. Ghodsi, *Sens. Actuators, A* **2013**, *195*, 71.
- [225] K. H. J. Buschow, *Handbook of Magnetic Materials*, Elsevier, Amsterdam, The Netherlands **2006**.
- [226] Nucleus Scientific, *X-Muscle Gen. 2*, Cambridge, Massachusetts, USA **2016**.
- [227] D. Villegas, M. V. Damme, B. Vanderborght, P. Beyl, D. Lefeber, *Adv. Rob.* **2012**, *26*, 1205.
- [228] G. Krishnan, J. Bishop-Moser, C. Kim, S. Kota, *J. Mech. Rob.* **2015**, *7*, 041014.
- [229] I. Tatsuzaki, K. Itoh, S. Ueda, Y. Shindo, *Phys. Rev. Lett.* **1966**, *17*, 198.
- [230] K. Uchino, *Mater. Res. Innovations* **1997**, *1*, 163.
- [231] K. Takagi, S. Kikuchi, J.-F. Li, H. Okamura, R. Watanabe, A. Kawasaki, *J. Am. Ceram. Soc.* **2004**, *87*, 1477.
- [232] B. Kundys, *Appl. Phys. Rev.* **2015**, *2*, 011301.
- [233] M.-F. Yu, O. Lourie, M. J. Dyer, K. Moloni, T. F. Kelly, R. S. Ruoff, *Science* **2000**, *287*, 637.
- [234] I. A. Levitsky, W. B. Euler, V. A. Karachevtsev, *Photophysics of Carbon Nanotubes Interfaced with Organic and Inorganic Materials*, Springer Science & Business Media, Springer-Verlag London **2012**, <http://www.springer.com/us/book/9781447148258>.
- [235] T. Ikeda, M. Nakano, Y. Yu, O. Tsutsumi, A. Kanazawa, *Adv. Mater.* **2003**, *15*, 201.
- [236] T. Hugel, N. B. Holland, A. Cattani, L. Moroder, M. Seitz, H. E. Gaub, *Science* **2002**, *296*, 1103.
- [237] H. Yu, *J. Mater. Chem. C* **2014**, *2*, 3047.
- [238] Y. Takashima, S. Hatanaka, M. Otsubo, M. Nakahata, T. Kakuta, A. Hashidzume, H. Yamaguchi, A. Harada, *Nat. Commun.* **2012**, *3*, 2280.
- [239] O. S. Bushuyev, M. Aizawa, A. Shishido, C. J. Barrett, *Macromol. Rapid Commun.* **2017**, *1700253*.
- [240] X. Lu, S. Guo, X. Tong, H. Xia, Y. Zhao, *Adv. Mater.* **2017**, *29*, 1606467.
- [241] *Molecular Magnets Recent Highlights* (Eds: W. Linert, M. Verdaguer), Springer, New York **2012**.
- [242] D.-Y. Kim, S. Shin, W.-J. Yoon, Y.-J. Choi, J.-K. Hwang, J.-S. Kim, C.-R. Lee, T.-L. Choi, K.-U. Jeong, *Adv. Funct. Mater.* **2017**, *27*, 1606294.
- [243] “Photothermal excitation for improved cantilever drive performance in tapping mode atomic force microscopy | Microscopy and

- Analysis," <http://www.microscopy-analysis.com/magazine/issues/photothermal-excitation-improved-cantilever-drive-performance-tapping-mode-atomic> (accessed: July 2017).
- [244] M. Karpelson, G.-Y. Wei, R. J. Wood, in *2008 IEEE International Conference on Robotics and Automation*, Pasadena, CA, USA **2008**, IEEE, p. 779.
- [245] T. Niino, S. Egawa, N. Nishiguchi, T. Higuchi, in *1992 Proc. IEEE Micro Electro Mechanical Systems*, IEEE, Travemunde, Germany **1992**, p. 122.
- [246] W.-C. Chuang, H.-L. Lee, P.-Z. Chang, Y.-C. Hu, *Sensors* **2010**, *10*, 6149.
- [247] M. D. Volder, D. Reynaerts, *J. Micromech. Microeng.* **2010**, *20*, 043001.
- [248] I. W. Hunter, J. M. Hollerbach, J. Ballantyne, *Rob. Rev.* **1991**, *2*, 299.
- [249] F. Daerden, D. Lefeber, *Eur. J. Mech. Environ. Eng.* **2002**, *47*, 11.
- [250] S. Kim, C. Laschi, B. Trimmer, *Trends Biotechnol.* **2013**, *31*, 287.
- [251] R. F. Shepherd, A. A. Stokes, J. Freake, J. Barber, P. W. Snyder, A. D. Mazzeo, L. Cademartiri, S. A. Morin, G. M. Whitesides, *Angew. Chem., Int. Ed.* **2013**, *52*, 2892.
- [252] V. Magdanz, M. Medina-Sánchez, L. Schwarz, H. Xu, J. Elgeti, O. G. Schmidt, *Adv. Mater.* **2017**, *29*, 1606301.
- [253] *Internal Document, Nucleus Scientific*, Cambridge, Massachusetts, USA **2016**.